ELSEVIER

Contents lists available at ScienceDirect

# Geochimica et Cosmochimica Acta

journal homepage: www.elsevier.com/locate/gca



# Modeling the impacts of diagenesis on carbonate paleoredox proxies

Kimberly V. Lau<sup>a,1</sup>, Dalton S. Hardisty<sup>b,1</sup>



<sup>a</sup> Department of Geosciences and Earth and Environmental Systems Institute, The Pennsylvania State University, University Park, PA, United States <sup>b</sup> Department of Earth and Environmental Sciences, Michigan State University, East Lansing, MI, United States

# ARTICLE INFO

Article history:
Received 19 March 2022
Accepted 17 September 2022
Available online 23 September 2022
Associate editor: Chao Li

Keywords: Carbonate geochemistry Diagenetic modeling Calcium isotopes

### ABSTRACT

The geochemistry of the carbonate sedimentary record is invaluable for understanding the ancient seawater evolution of carbon and redox-sensitive elements. However, the application of carbonate geochemical paleoredox proxies can be limited by our ability to recognize records impacted by syn- and postdepositional diagenesis with pore fluids that have geochemical compositions which are distinct from the overlying seawater-resulting from variable redox conditions, fluid sources, and sediment- vs seawater-buffered conditions. We extend a numerical framework, established for the application of Ca isotopes, for recognizing sediment- vs fluid-buffered alterations during aragonite-to-calcite recrystallization for widely applied carbonate paleoredox proxies: iodine ratios (I/Ca), cerium anomaly (Ce/Ce\*), and carbonate-associated Cr, U, and S isotopes. We model endmember reducing and oxidizing fluid diagenetic scenarios, as opposed to incorporating biogeochemical evolution of pore fluids within the model. The results reveal that early, fluid-buffered diagenesis of relatively unevolved seawater ("seawater-buffered") represents the ideal scenario for preservation for all proxies, including C isotopes. Conversely, fluidbuffered alteration in pore fluids with redox conditions highly evolved from the overlying water column is likely to alter the primary carbonate geochemistry. Model calibration against records from the Bahamas Clino and Unda cores suggests each proxy is uniquely sensitive to a given style of diagenetic alteration, with Ce/Ce\* the most robust and I/Ca ratios most sensitive to early diagenetic alteration. We recommend multiple strategies, including relationships with C, O, and Ca isotope data, that can be leveraged to identify the preservation of primary seawater geochemistry for a given proxy. Last, we compare the diagenetic model predictions with published records from the Permian/Triassic boundary to demonstrate how incorporating stratigraphic geochemical patterns alongside interpretation of diagenetic model results can support interpretation of secular seawater signals. To improve our understanding of the effects of diagenesis on carbonate paleoredox proxies, additional experimental constraints, fieldbased observations, and multi-proxy datasets are needed.

© 2022 The Authors. Published by Elsevier Ltd. This is an open access article under the CC BY-NC-ND license (http://creativecommons.org/licenses/by-nc-nd/4.0/).

# 1. Introduction

Oxygenation and deoxygenation of the oceans strongly influence organic carbon burial, habitability for marine biota, and biogeochemical cycling of nutrients and critical redox-sensitive elements. Inorganic geochemical proxies—a broad category that includes concentrations of redox-sensitive elements and their isotopic ratios—offer the potential to track redox conditions across a range of temporal and spatial scales. Our understanding of the evolution of oxygen and related redox-sensitive elements critical for life is dominantly shaped by records of carbonate geochemistry for much of Earth history. Carbonate mineral precipitation can be

directly linked to seawater chemistry, and deposition of carbonate minerals has been nearly continuous since 3.8 billion years ago (Krissansen-Totton et al., 2015). Therefore, redox proxies measured in carbonates have been critical for understanding long-term change across the Precambrian and Phanerozoic as well as transient perturbations. For example, the carbon isotope composition of carbonate rocks ( $\delta^{13}C_{\text{carb}}$ , simplified here to  $\delta^{13}C$ ) can reflect the balance of organic carbon burial, oxidation, and production via photosynthesis, which contributes to the production and accumulation of oxygen in Earth's atmosphere and ocean over time (Hayes and Waldbauer, 2006). In combination with  $\delta^{13}C$ , other redox-sensitive elements in carbonates such as I, Ce, Cr, U, S—which are progressively sensitive to more reducing conditions (Fig. 1)—together provide constraints on atmosphere–ocean oxygen concentrations and the relative redox potential (Eh) of

<sup>&</sup>lt;sup>1</sup> These authors contributed equally to this work. *E-mail addresses*: kvlau@psu.edu (K.V. Lau), hardist1@msu.edu (D.S. Hardisty)

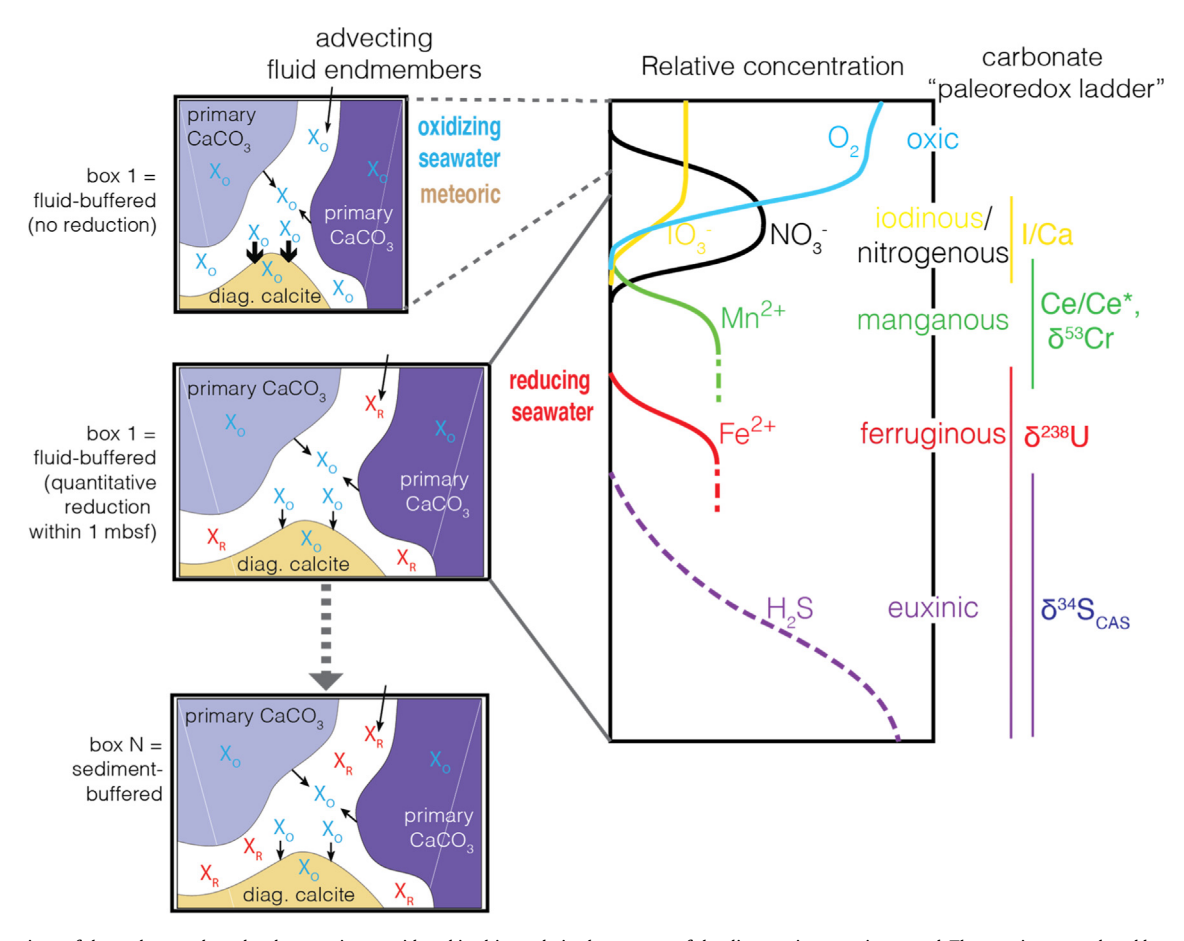


**Fig. 1.** Comparison of the carbonate-based redox proxies considered in this study in the context of the diagenetic scenarios tested. The proxies are ordered based on the redox potential most closely linked to the reduction of the oxidized species of each proxy. For example, U reduction occurs close to the Fe(III)-Fe(II) redox potential but its reduction also reflects the amount of sulfide that is present (e.g., Bruske et al., 2020). The boxes to the left depict the geochemical reactions impacting a redox-sensitive proxy, X, where  $X_0$  (blue) represents the oxidized species and  $X_R$  (red) represents the reduced species. During diagenesis,  $X_0$  is released into the pore fluid and is mixed with solutes from the diagenetic fluid, and subsequently can be taken up into the diagenetic calcite. The oxidizing seawater and meteoric diagenetic scenarios are limited to fluid-buffered conditions (i.e., box = 1), whereas the reducing seawater diagenetic scenario assumes that reduction occurs in the first box (in the first 1 m) with recrystallization reactions continuing along the flow path (i.e., to box = N). (For interpretation of the references to colour in this figure legend, the reader is referred to the web version of this article.)

the oceans, oxidative weathering, global vs regional/local marine redox gradients, relative timing of environmental events, and the cycling of redox-sensitive elements critical to biological evolution (Algeo and Li, 2020).

The unique redox sensitivity and global vs regional environmental conditions captured by the I/Ca, Ce/Ce\*,  $\delta^{53}$ Cr,  $\delta^{238}$ U, and  $\delta^{34}S_{CAS}$  paleoredox proxies make their combined application particularly useful (Fig. 1). The global vs local sensitivity of an individual proxy is defined by a combination of the redox-sensitive speciation or redox-sensitive isotope fractionation as well as the residence time of the given element relative to ocean mixing times (Table 1). Using these criteria, I/Ca,  $\delta^{53}$ Cr, and Ce/Ce\* reflect local/ regional paleoredox conditions whereas the modern ocean residence times of U and S allow for relatively homogenous marine isotopic signatures and hence have the potential to record global marine redox conditions. Further, the proxies can fingerprint different Eh thresholds: to illustrate, the  $\delta^{34}S$  of seawater sulfate is driven largely by the proportion of seafloor characterized by sulfidic conditions (e.g., Gill et al., 2011; Owens et al., 2013) whereas seawater  $\delta^{238}$ U is sensitive to anoxic (ferruginous)/euxinic conditions at the seafloor (e.g., Brennecka et al., 2011; Lau et al., 2016; Zhang et al., 2018: Gilleaudeau et al., 2019), Both  $SO_4^{2-}$  and U(VI) species undergo isotopic fractionation during reduction in anoxic settings, representing a major sink for sequestering the isotopically fractionated S and U. Variations in reducing sinks are reflected in the isotope compositions of seawater that can subsequently be recorded in carbonate minerals. Other factors that must also be considered in interpreting seawater values, beyond the extent of seafloor anoxia and associated organic carbon burial, include the reservoir size and residence time, spatial redox heterogeneities (Li et al., 2017), and changes in the riverine fluxes (Canfield, 2013; Chen et al., 2021).

A critical challenge for interpreting inorganic geochemical proxies, including paleoredox applications, is determining whether the geochemistry of carbonates faithfully reflects the seawater from which it precipitated. Stratigraphic variations in carbonate geochemical proxy records can also be interpreted as changes in carbonate geochemical preservation (e.g., syn- and post-depositional diagenesis or the lack thereof) from exposure to evolved marine, meteoric, or burial pore fluids. To investigate this alternative interpretation, a series of carbonate proxies, such as I/Ca, rare earth elements (Ce/Ce\*) and isotopes of C, O, U, Li, S, Ca, Mg, B, Cr, have been evaluated from two Neogene-to-Recent cores (Clino and Unda) from the Great Bahama Bank, among other locations (Chen et al., 2018; Dellinger et al., 2020; Hardisty et al., 2017; Higgins et al., 2018; Melim et al., 1995; Murray et al., 2021; Oehlert and Swart, 2014: Oehtert and Swart. 2019: Stewart et al., 2015: Swart et al., 2001: Tissot et al., 2018: Wang et al., 2021). For most of the studied sites, variations in geochemical records can be attributed to diagenesis or other factors not related to evolving seawater redox

**Table 1**Comparison of marine chemical composition and associated parameters associated with the paleoredox proxies of interest to this study. See Table 2 for detailed references.

Proxy	Species expected in carbonate minerals	Typical marine concentration of aqueous species	Marine isotope composition (‰)	Ocean residence time (years)
I/Ca	$I(V)O_3^-$	460 nmol/kg	NA	340,000
Ce/Ce* δ <sup>53</sup> Cr	Ce(IV)CO <sub>3</sub> <sup>+</sup>	5 pmol/kg	NA	50-130
$\delta^{53}$ Cr	$Cr(VI)O_4^{2-}$ , $Cr(III)$ species if reducing	4 nmol/kg	0.91 ± 0.36	8,000
$\delta^{238}U$	$U(VI)O_2(CO_3)_3^{4-}$ , $U(IV)$ species if reducing	13.4 nmol/kg	-0.39	400,000
$\delta^{34}S_{CAS}$	S(VI)O <sub>4</sub> <sup>2-</sup>	28 mmol/kg	20.8-22.0	8,700,000

conditions. The published data from the well-oxygenated Great Bahama Bank, from the studies listed above, capture a range of diagenetic environments (meteoric, marine, burial), diagenetic styles (fluid- vs sediment-buffered), and diagenetic processes (aragonite-to-calcite neomorphism/stabilization, recrystallization, dolomitization) over the late Neogene. A key finding from these studies is that, while preservation of primary, seawater-derived oxic signals is possible under certain circumstances, signals indicative of anoxic or low-oxygen water-column states are instead attributed to diagenesis and mixing of sediment sources. The conclusion that carbonate redox proxies are not always faithful recorders of seawater chemistry is supported by other approaches, such as variability in  $\delta^{34}S_{CAS}$  and  $\delta^{238}U$  across microfacies and sedimentary components (Present et al., 2015, 2019,2020; Hood et al., 2016, 2018; Richardson et al., 2019; Murray et al., 2021).

In parallel to these field-based studies, numerical models have been developed to recognize specific diagenetic conditions that determine which carbonate samples may preserve ancient seawater signals (Jacobsen and Kaufman, 1999; Ahm et al., 2018; Zhao et al., 2020). Diagenetic models can predict the trajectory of solid geochemical evolution occurring during early burial and in exchange with seawater (i.e., fluid-buffered) or in chemically evolved pore fluids that are relatively isolated from exchange with seawater (i.e., sediment-buffered) conditions. The results suggest the potential for coupling paleoenvironmental proxies with isotopic diagenetic indicators (e.g., Ca and Mg isotopes) to assess samples or stratigraphic intervals that are most likely to preserve primary redox signals (Higgins and Schrag, 2012; Fantle and Higgins, 2014; Blättler et al., 2015; Husson et al., 2015). For example, a coupled Ca-Mg isotope approach has been used to recognize fluid- vs sediment-buffered dolomite, respectively, for applications of Li, C, and S isotope values, to constrain ancient seawater chemistry (Ahm et al., 2018, 2019, 2021; Bold et al., 2020; Jones et al., 2020; Crockford et al., 2021; Nelson et al., 2021; Bryant et al., 2022). However, diagenetic models of Ca-Mg isotopes have not been systematically applied to paleoredox proxies.

Recognizing how and when carbonates retain seawater geochemical signals relies on understanding the sensitivity of the individual proxy to diagenetic alteration under various conditions and our ability to constrain the likelihood that these conditions occurred. To this end, we constructed diagenetic models for a series of paleoredox proxies commonly applied to carbonates— $\delta^{13}$ C, I/Ca, Ce/Ĉe\*,  $\delta^{53}$ Cr,  $\delta^{238}$ U, and  $\delta^{34}$ S—and focus on relative changes in these proxies with diagenesis. The models consider meteoric and marine diagenesis with endmember oxidizing and reducing conditions and are used to constrain the early diagenetic conditions that best preserve seawater values for each proxy. This suite of paleoredox proxies has been evaluated in the same set of carbonate samples from the Bahamas (Clino and Unda cores, among others) that have experienced well-constrained postdepositional alteration, providing a basis for ground-truthing the model. Using these model insights, we evaluate interpretations of paleoredox records in the carbonate record.

### 2. Overview of carbonate geochemical proxies

The proxy suite evaluated in this study can be grouped into two broad, non-exclusive categories; paleoredox and diagenetic proxies. Because these proxies have been each studied intensively, we refer to published reviews for a more detailed overview. The carbonate paleoredox proxies include iodine-to-calcium (I/Ca) ratios (Hardisty et al., 2017; Lu et al., 2020), the cerium anomaly (Ce/Ce\*; Liu et al., 2019; Tostevin, 2021), carbonate-associated chromium isotopes ( $\delta^{53}$ Cr; Bauer et al., 2021; Wang et al., 2021), carbonate-associated uranium isotopes ( $\delta^{238}$ U; Chen et al., 2018; Lau et al., 2019), and carbonate-associated sulfur isotopes (CAS and  $\delta^{34} S_{CAS}$ ; Murray et al., 2021; Bryant et al., 2022). The diagenetic proxies include calcium isotopes (44Ca/40Ca, reported in delta notation as  $\delta^{44}$ Ca relative to modern seawater; Higgins et al., 2018), magnesium isotopes ( $\delta^{26}$ Mg; Tipper, 2022), strontium-to-calcium ratios (Sr/Ca), carbon isotopes ( $\delta^{13}$ C; Ahm and Husson, 2021), and oxygen isotopes ( $\delta^{18}$ O). Although the CaCO<sub>3</sub> mineral polymorphs aragonite and high-Mg calcite (HMC) represent a significant contribution to sediments today (Swart and Eberli, 2005) as well as throughout Earth history (Hardie, 1996; Stanley and Hardie, 1998), they are ubiquitously transformed to more stable low-Mg calcite (LMC) or dolomite. Therefore, this study focuses on the alteration of metastable aragonite to stable LMC and links the composition of redox-sensitive elements in the diagenetic calcite to: (1) the redox state of the diagenetic fluid, (2) the source and associated composition of the diagenetic fluid, and (3) the mechanisms of solute transport (i.e., advection) and reaction that determine fluid- vs sediment-buffered conditions.

Because redox-sensitive elements represent trace, nonstoichiometric constituents of aragonite and LMC and will undergo chemical transformations in reducing pore waters, their isotopic compositions are susceptible to alteration. The extent of alteration is influenced by the degree of sediment- vs fluid-buffered conditions as well as the chemical compositions of the pore fluids, which can vary widely from that of primary seawater. The redox state of the diagenetic fluids must be considered because it can alter the availability of the redox species with the highest affinity for incorporation into LMC (Table 1). Importantly, the sensitivity of these redox species to progressively reducing conditions is also manifested in sediment porewaters. In organic-rich porewaters, redoxactive elements are sequentially reduced during the oxidation of organic matter-with overlaps common in their respective 'zones'-in an order dictated by their relative availability and predicted by thermodynamics (Fig. 1: Froelich et al., 1979; Canfield and Thamdrup, 2009). While these reduction reactions are sequential, they can all occur within the upper few cm's of the sediment and in some cases proceed nearly quantitatively. For example, while sulfate reduction may occur over the upper few meters of reducing sediment columns (Lyons et al., 2004), the reduction of IO<sub>3</sub>, Ce(IV), Cr(VI), and U(VI) can be complete in the upper few cm's (Kennedy and Elderfield, 1987a,b; Algeo and Li, 2020). For the isotope-based proxies, this reduction may impart isotope fractionations to varying degrees into recrystallized or diagenetic LMC depending on the relative resupply of unaltered seawater to pore fluids, which typically diminishes with increasing depth below the sediment–water interface.

A framework for applying multiple diagenetic proxies to identify scenarios where the primary carbonate compositions are preserved has been developed using measurements of  $\delta^{44}$ Ca,  $\delta^{26}$ Mg, and/or Sr/Ca in combination with numerical models (Fantle and Higgins, 2014; Blättler et al., 2015; Ahm et al., 2018; Higgins et al., 2018). This approach is based on the premise that the formation of diagenetic carbonate minerals (dolomite, LMC) can occur under both sediment- and fluid-buffered conditions with respect to a given element-i.e., evolved pore fluids versus seawater (Higgins and Schrag, 2010, 2012; Fantle and Higgins, 2014; Blättler et al., 2015; Husson et al., 2015). For Ca specifically, diagenesis in a fluid-buffered system causes the  $\delta^{44}$ Ca value of the carbonate to evolve toward the  $\delta^{44}$ Ca of the pore fluid (Fantle and DePaolo, 2007). When recrystallization occurs in a sedimentbuffered system, the  $\delta^{44}$ Ca value of the diagenetic carbonate is buffered by the  $\delta^{44}$ Ca value of the precursor carbonate—and hence remains relatively unchanged. For Sr, diagenetic calcite is generally characterized by lower concentrations (Sr/Ca < 1 mmol/mol) in comparison to primary aragonite (Sr/Ca ~ 10 mmol/mol; Kinsman and Holland, 1969; Banner, 1995). Similarly, lower Mg incorporation in diagenetic calcite results in lower Mg/Ca ratios relative to primary aragonite and higher  $\delta^{26}$ Mg values due to the large isotope fractionation associated with calcite precipitation. Therefore, data and model results indicate that paired measurements of bulk sediment  $\delta^{44}$ Ca values vs Sr/Ca ratios and/or  $\delta^{26}$ Mg serve as robust geochemical signatures to identify LMC recrystallized from aragonite under sediment vs fluid-buffered early marine diagenesis—i.e., low vs high  $\delta^{44}$ Ca, respectively, in combination with low Sr/Ca and high  $\delta^{26}{\rm Mg}$  (Husson et al., 2015; Lau et al., 2017; Ahm et al., 2018; Higgins et al., 2018; Gussone et al., 2020).

The  $\delta^{13}$ C and  $\delta^{18}$ O tracers are also useful indicators for diagenesis. The sequential reduction of the redox-sensitive elements during early diagenesis is driven by organic matter remineralization, which produces porewater dissolved inorganic carbon (DIC) with  $\delta^{13}$ C values lower than seawater. Similar to  $\delta^{44}$ Ca, the  $\delta^{13}$ C of the diagenetic LMC may be buffered by the  $\delta^{13}$ C value of the precursor carbonate during sediment-buffered conditions, but fluid-buffered conditions can result in carbonate that deviates from these values toward the composition of the porewaters. Comparatively,  $\delta^{18}$ O is a sensitive tracer of interactions with meteoric fluids with lower  $\delta^{18}$ O values than seawater-derived fluids and carbonates (Melim et al., 1995; Swart and Oehlert, 2018).

#### 3. Methods

This study aims to simulate bulk carbonate sediments that are representative of shallow marine carbonate environments, where the primary carbonate minerals reflect seawater-derived and predominantly biotically driven precipitation from both an initially oxic and an initially anoxic water column. We model the early diagenetic alteration expected during recrystallization of bulk carbonate sediments (99% aragonite, 1% HMC) to stable LMC with three different diagenetic fluid compositions: oxidizing seawater, (oxidizing) meteoric, and reducing seawater-derived fluids. The distinction between oxidizing and reducing fluids is that oxidizing conditions are sufficiently abundant in the oxidized redox species that the solid geochemistry of the redox-sensitive elements is controlled not by reduction but instead reflect element partitioning and isotope fractionation between primary and diagenetic carbonate minerals. We do not consider dolomitization because the

behavior of redox-sensitive elements for dolomite is poorly constrained.

We do not model biogeochemical evolution of fluids (i.e., oxidizing fluids remain oxidizing) nor do we explicitly prescribe a dissolved O<sub>2</sub> concentration in these fluids. Instead, we chose to model endmember oxidizing and reducing fluids for the following reasons. (1) There is a lack of observational and experimental data for iodine, chromium, uranium, and cerium in carbonatedominated sediments necessary for modeling their reduction kinetics, but their geochemistry in reducing vs oxidizing sediments is better characterized (see Table 2). (2) Iodine, chromium, uranium, and cerium have high reduction potentials and are relatively limiting relative to organic matter and sulfide—a strong reductant for most of these systems-and are thus reduced on the scale of cm's during early diagenesis. Given that the model domain, described below, is of relatively coarse resolution (a series of 1 m<sup>3</sup> boxes), it is expected that quantitative reduction of these elements would occur within box 1 near the sediment-water interface, and thus modeling the reduction reactions is unnecessary. (3) Modeling endmember fluid compositions allows for the versatility to consider scenarios where the overlying seawater is either reducing or oxidizing, which is relevant to ancient oceans.

#### 3.1. Numerical models of carbonate geochemical diagenesis

We adapt the water–rock interaction model from Jacobsen and Kaufman (1999) and the diagenetic model from Ahm et al. (2018). Common to both models is no change in porosity (i.e., no net dissolution or net precipitation), in contrast to reactive transport models (Fantle et al., 2020; Zhao et al., 2020) that can incorporate burial of new minerals during deposition. Reactive transport models can also account for changes in porewater carbonate chemistry and alkalinity that result from microbial respiration reactions, which can impact diagenetic rates and the net precipitation of new authigenic carbonates—feedbacks not considered in our models. Last, the more generalized diagenetic models that are employed in this study do not consider the effect of sedimentation. Model equations are described in the Supplementary Material.

Water-rock interaction models of diagenesis can be used to evaluate the sensitivity of a given geochemical component of a solid to alteration with various diagenetic fluid compositions and water-rock ratios. This approach approximates the geochemical change during recrystallization for a fluid-to-rock mass ratio,  $(\eta = F(1 - F))$ , where F is the mass fraction of fluid in the system) and reflects the degree of disequilibrium between the solid and fluid (e.g., Banner and Hanson, 1990; Jacobsen and Kaufman, 1999). The single-element partition coefficient ( $D_i = C_s/C_f$ , where the concentration of the element of interest, i, in the solid is  $C_s$ and in the fluid is  $C_f$ ) determines the extent of geochemical change from initial values for a given water-rock ratio (Fig. 2). The solid isotopic composition ( $\delta_s$ ) reflects the new equilibrium at a given water-rock ratio by applying an isotope fractionation factor ( $\alpha$ , converted to  $\Delta = 1000(\alpha - 1)$ ) to the fluid isotope composition  $(\delta_f)$ . This approach can model closed vs open systems: in the former, the diagenetic solid composition reflects the redistribution of elements between the fluid and solid at a given water-rock ratio, whereas the latter accounts for the evolution of the solid geochemistry with alteration. Here, we use the equations from Jacobsen and Kaufman (1999) for open systems.

Although these water–rock models are useful for encapsulating the first-order impact of water–rock interactions, they are less ideal for evaluating the ultimate endmember geochemical signatures of the diagenetic composition because the fluid geochemistry is prescribed and does not evolve during diagenesis from primary mineral (aragonite) dissolution, i.e., the models have no fluid-rock reaction component.

 Table 2

 Model geochemical parameters and geochemical values. Please refer to Supplementary Material for explanation of footnotes and more detailed discussion.

Parameter Definition		Definition	С	O	Ca	Mg	Sr	I	Ce	Cr	U	S
Primary aragonite – oxic water column	C <sub>s,o</sub> (mg/kg)	Initial solid conc.	120000 [1]	480000 [1]	387500 [2]	2500 [2]	10000 [2]	6 [5]	0.4535 [6]	Mixed – 3 Cr(VI) only – 1.0 /8/	Mixed – 4.1 [3] U(VI) only – 3 [3,4]	3765.5 [7]
	δΙ <sub>s,o</sub> (‰)	Initial solid isotope value	5 [2,9]	-0.5 [2]	-1.6 [1,10]	-1.7 [11]	NA	NA	0.67 [6]	Mixed – 0.8 Cr(VI) only – 0.56 [8, 12]	Mixed0.15 U(VI) only0.37 [3,4]	22 [13]
Primary calcite – oxic water column	C <sub>s,o</sub> (mg/kg)	Initial solid conc.	Same as aragonite		394500 [2]	5000 [2]	500 [2]	Same as arag.	0.4535 [6]	Same as aragonite	0.64 [3,4]	Same as aragonite
	δI <sub>s,o</sub> (‰)	Initial solid isotope value	3.2 [14]	Same as arag.	-1.1 [2]	-3.8 [2,11]	NA	NA	Same a	as aragonite	-0.37 [3,4]	24 [7]
Primary aragonite and calcite – anoxic water column	C <sub>s,o</sub> (mg/kg)	Initial solid conc.			Same as o	xic		<1 ppt [15]	Same as oxic	20 [8]	6.1 [3,4]	110 [16]
	$\delta I_{s,o}(\%)$	Initial solid isotope value		Samo	e as oxic		NA	NA	1.025 [6]	1.6 [8]	0.21 [17]	38.4 [7]
Diagenetic calcite	α	Fractionation factor	1.001 [2]	1.0330 [2]	1.0 [1]	0.998 [1,18]	NA	NA	1.0 [19]	Mixed – 0.99954 [20] Cr(VI) only – 0.99930 [12]	Seawater – 1.00025 Meteoric – 1.00003	Oxidizing – 1.0017 Reducing – 1.003 [21]
	K <sub>D</sub> or stoichio- metry	Partition coefficient, mineral stoichiometry	120 [22]	5.5E-5 [22]	1 Ca:C – 0.965	0.0014 Mg:C - 0.035	0.025 [23]	Seawater – 0.1317 Meteoric – 0.0064 [24]	198 [25]	11 [26]	Oxidizing – 1.031 Reducing –18.8 [4] U(VI) only – 0.209 [27]	3.6E-4 [28]
Oxidizing seawater	C <sub>f,o</sub> (mol/kg)	Initial fluid conc.	0.002 [29]	NA	0.01028 [29]	0.0533 [29]	0.00009 [29]	0.3750E-6 [30]	1.3132E- 11 <i>[6]</i>	2.85E-9 [31]	1.3444E-8 <i>[32]</i>	0.028 [33]
	δI <sub>f,o</sub> (‰)	Initial fluid isotope value	-2 [2]	-30.5 [2]	0 [10]	-0.8 [10]	NA	NA	0.46 [6]	1.26 [8, 20]	-0.39 [4]	21[34]
Meteoric/ groundwater	$\begin{array}{c} C_{f,o} \\ (mol/kg) \end{array}$	Initial fluid conc.	0.0012 [35]	NA	0.002 [35]	0.0049 <i>[36]</i>	2.5E-6 [35]	2.5091E-7 <i>[37]</i>	3.6042E-9 [38]	149.8E-9 <i>[39]</i>	4E-9 [40]	190E-6 [41]
	$\delta I_{f,o}$ (‰)	Initial fluid isotope value	-3.245 <i>[33]</i>	-37.7 [42]	-1.095 [43]	-1.09 [36]	NA	NA	1.395 [44]	0.49 [45]	-0.30 [4]	5.5 [46]
Reducing seawater	$\begin{array}{c} C_{f,o} \\ (mol/kg) \end{array}$	Initial fluid conc.	0.0024 <i>[47]</i>	NA	0.01028 [29]	0.0533 [10]	0.00009 [29]	7.8802E-15 <i>[48]</i>	6.4297E- 09 <i>[49]</i>	2.5E-9 [50]	1.428E-9 <i>[3]</i>	0.010 [51]
	δI <sub>f,o</sub> (‰)	Initial fluid isotope value	-10 [47]	-30.5 [2]	0 [10]	-0.8 [10]	NA	NA	1.025 [52]	1.6 [50]	0.21 [17]	35.4 [53]

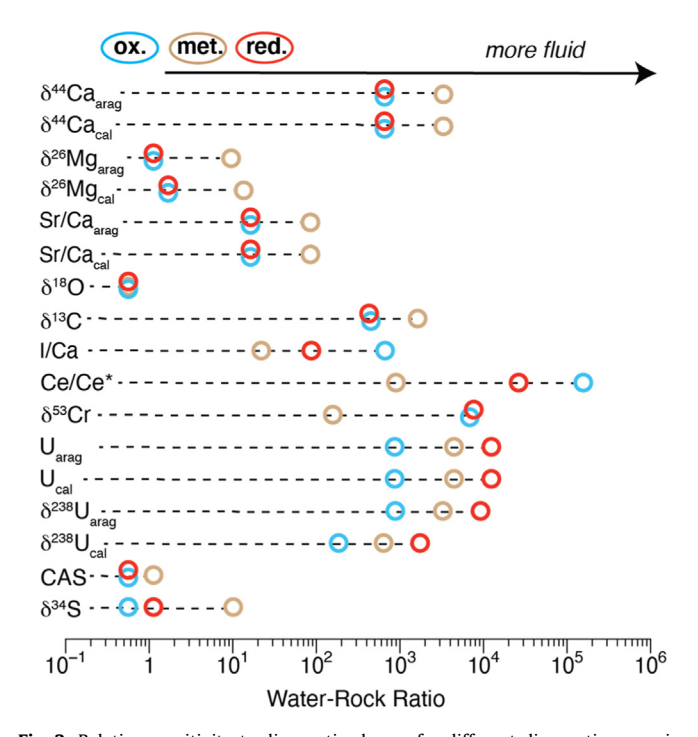


**Fig. 2.** Relative sensitivity to diagenetic change for different diagenetic scenarios from water-rock modeling. The water-rock ratio at which a geochemical proxy has been altered halfway between its initial and final composition is shown. Subscript "arag" indicates primary aragonite and subscript "cal" indicates primary calcite, both precipitated from an oxidizing water column. Ox. = oxidizing seawater, met. = meteoric fluid, red. = reducing seawater. (For interpretation of the references to colour in this figure legend, the reader is referred to the web version of this article.)

In contrast, diagenetic models, such as that developed by Ahm et al. (2018), explicitly consider sediment-buffering of the diagenetic fluid, mineral reaction rates, and fluid advection rates, and thus are a powerful tool for evaluating alteration with more realistic fluid-rock reactions. Analogous to previous studies, the model domain consists of 40 sequential 1 m<sup>3</sup> sediment packages, where fluid flows from outside the model domain into box 1 and progressively reacts with the sediment. Box 1, which represents the sediment in contact with seawater, is akin to an open system ("fluid-buffered") whereas box 40 is described as "sediment-buff ered" because the fluid geochemistry has the potential to have been altered away from the original composition due to reaction. leaving the bulk carbonate  $\delta^{44}$ Ca value relatively unchanged from the primary values (see supplementary discussion for details on defining sediment buffered). Unlike the water-rock models, the sensitivity of a proxy to geochemical change is not evaluated in this diagenetic model because the water-rock ratio is a function of the advection of the diagenetic fluid and of the reaction rate that determines the proportion of sediment that is recrystallized at each time step, and not simply the geochemical disequilibria between the solid and the fluid.

# 3.2. Selection and justification of values of model parameters

Previous application of these diagenetic models has focused primarily on the major elements in carbonate minerals (e.g., Ca, Mg, C, O). In this study, we focus on the trace, redox-sensitive elements whose concentrations in carbonate minerals are prescribed with a  $K_D$ . The parameter values for their selection are presented in Table 2 (see detailed description and justification in the Supplementary Materials). The same parameterization is used for simulations with both models. When applicable, we used the same

parameter values for C, O, Ca, Mg, and Sr from Ahm et al. (2018). The Cr, U, and S isotope proxies have been previously implemented in diagenetic models (Chen et al., 2018; Wang et al., 2021; Bryant et al., 2022), and, when applicable, similar values are used here. A detailed discussion of assumptions regarding the coprecipitation of U and S valence states is in the Supplementary Materials (Fig. S8). A comparison of our endmember S model (which does not explicitly simulate sulfate reduction) to model results from Bryant et al. (2022), which implemented a fixed sulfate reduction rate to simulate sulfate evolution along a reaction flow path, is provided in the Supplementary Materials (see Fig. S4). The I and Ce/Ce\* proxies have not been included in similar diagenetic models and our modeling for other redox proxies includes diagenetic conditions beyond those considered in previous studies. For these scenarios, we estimated parameter values based on experimental or observational data: future updates or revisions to these values can be accommodated in the model using the code that is available at https://doi.org/10.2627/wrdz-sz05.

The model was designed to simulate diagenesis in shallow carbonate platform environments, from which most constraints in modern or Recent carbonate sediments are derived. In contrast, carbonate sediments in pelagic environments that are dominated by planktonic calcite may exhibit different initial compositions and diagenetic parameters (i.e., reaction rate, advection, porosity).

### 4. Results

In this paper, we refer to "oxidizing" as oxidizing with respect to the redox species incorporated into carbonate and hence this condition is specific to each redox proxy. "Reducing" refers to reducing with respect to the redox species incorporated into carbonate and is similarly unique for each redox proxy. "Fluidbuffered" conditions refer to box 1 of the model domain where significant seawater or meteoric contributions limit porewater geochemical evolution related to carbonate dissolution (Ahm et al., 2018; Bryant et al., 2022). "Seawater-buffered" refers to fluidbuffered conditions where the pore fluid redox state is analogous to that of the overlying water column from which the primary aragonite is derived with respect to the proxy of interest. "Sediment-buffered" conditions are defined with respect to  $\delta^{44}$ Ca and refer to box 40 of the model, where the diagenetic fluid has undergone significant geochemical evolution from primary seawater because of progressive carbonate dissolution in overlying sediments and the sediment  $\delta^{44}$ Ca is relatively unchanged (see discussion in Supplementary Material and Fig. S1).

# 4.1. Impacts of water–rock ratios and fluid chemistry on carbonate geochemistry

Water-rock models can compare the degree to which a chemical system under given fluid-rock conditions can resist geochemical change and best preserve its original composition. Figs. 2 and S1 show the model results for open-system diagenesis with oxidizing seawater, meteoric fluids, and reducing seawater. Like previous modeling,  $\delta^{18}$ O is altered at very low water-rock ratios because oxygen is poorly buffered in the carbonate compared to its availability in water. Under meteoric diagenesis, alteration occurs at higher water-rock ratios for most proxies except for I/Ca, Ce/Ce\*, and  $\delta^{53}$ Cr. For the  $\delta^{53}$ Cr and U proxies, diagenetic resetting with reducing seawater occurs at higher water-rock ratios.

We also compare the diagenetic trajectories for  $\delta^{44}$ Ca,  $\delta^{26}$ Mg, Sr/Ca, U concentrations, and  $\delta^{238}$ U if HMC or aragonite is the initial CaCO<sub>3</sub> polymorph. Aragonite tends to have lower  $\delta^{44}$ Ca and higher [Sr] and [U] (Kinsman, 1969; Meece and Benninger, 1993; Gussone et al., 2005) and therefore requires higher water–rock ratios to be

altered compared to calcite for these systems. The  $\delta^{44}$ Ca and Sr/Ca of aragonite-dominated sediments would also be expected to exhibit a larger difference between the initial and the reset value, whereas U concentrations would be expected to be more tightly constrained (Fig. S2).

# 4.2. Geochemical signatures of fluid- and sediment-buffered early marine diagenesis

The goals of this study are to (1) evaluate the conditions which best preserve primary seawater signatures during aragonite-to-calcite recrystallization for an individual proxy and (2) determine the potential to identify diagenetic conditions using additional geochemical signatures. To this end, we compared the extent of alteration of primary aragonite precipitated from both oxidizing and reducing seawater during its transformation to LMC in meteoric fluid-buffered diagenesis, reducing and oxidizing seawater fluid-buffered diagenesis, and reducing seawater sediment-buffered diagenesis (Fig. 3).

We calculated the percent of change from the initial elemental ratio, delta value, or calculated anomaly based on modern aragonite (Fig. 3). We note that the calculated % deviation will change if primary aragonite geochemistry or diagenetic fluid chemistry differs from today or from the values considered here. We highlight below key observations from Fig. 3 as well as the trajectories for diagenetic alteration shown in Figs. 4–6 that guide the subsequent discussion:

- 1. For nearly all the paleoredox proxies, fluid-buffered diagenesis with analogous redox states between the diagenetic fluid and the overlying water column—or "seawater-buffered"—is the best-case-scenario for preserving near-seawater geochemical compositions in diagenetic calcite (Figs. 3–6).
- 2.  $\delta^{13}$ C preservation may occur under "seawater-buffered" conditions only if porewater DIC and  $\delta^{13}$ C are relatively unevolved (see sensitivity analysis in Fig. S7).
- 3. The  $\delta^{238}$ U,  $\delta^{53}$ Cr, and Ce/Ce\* proxies have high preservation potential in sediment-buffered conditions even if the fluid redox state is opposite to that of the water column (Fig. 3).
- 4. There are large differences for the paleoredox proxies, including  $\delta^{13}$ C, in diagenetic calcite precipitated under oxidizing vs reducing fluid-buffered conditions.
- 5. For  $\delta^{34}$ S, prescribing endmember oxidizing vs reducing seawater geochemistry produces comparable results to implementing a fixed-reduction rate for sulfate reduction (Bryant et al., 2022; see Supplementary Material and Fig. S4). Minor differences are within the range of natural observations (Tromp et al., 1995) and arise from tuning the reduction rate in Bryant et al. (2022) to the sulfur cycle for Permian seawater, which is distinct from the modern (i.e., lower sulfate concentrations of 5 mmol/kg relative to 28 mmol/kg today).
- 6. Both the  $\delta^{26}$ Mg values and Sr/Ca ratios are similarly impacted by all styles of diagenesis during aragonite-to-calcite recrystallization. This reduces the utility of these proxies for recognizing specific styles of diagenesis and diagenetic fluids. As a result, we hereafter do not consider these proxies in our cross-plots and detailed discussions.
- 7. Apart from  $\delta^{34}$ S, each of the paleoredox proxies exhibit large deviations between primary aragonite and meteoric diagenetic calcite. This is because the geochemistry of meteoric fluids is highly variable compared to seawater and because these proxies are trace constituents of carbonate and therefore are not readily rock buffered (Fig. 2 and Fig. 3, brown bars). For details regarding the impact of fluid advection rates on model endmembers, see the sensitivity analysis in Figs. S5 and S6 and related supplementary discussion.

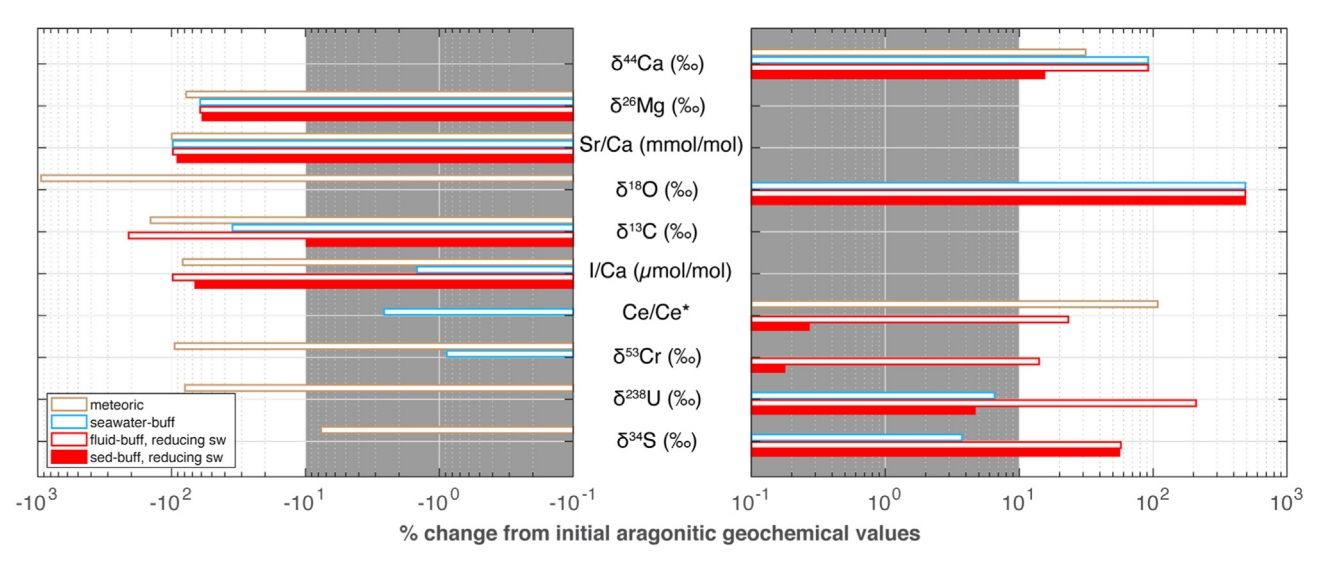


**Fig. 3.** Relative deviations from initial geochemical compositions for the considered proxies following diagenesis with meteoric fluids (brown), oxidizing seawater-buffered (open blue), and reducing seawater under fluid-buffered (open red) and sediment-buffered (solid red) conditions. These results simulate diagenesis of primary aragonite derived from an oxidizing water column. Units vary by proxy. Positive changes imply an increase and negative changes a decrease in proxy value. Changes > 100% imply that the magnitude of change exceeds that of the magnitude of the initial value. The grey zone is <10% change from the initial, aragonite-dominated composition—a change with limited impact on paleoredox interpretations for most proxies given analytical uncertainty, typical stratigraphic variability, and interpreted redox thresholds. (For interpretation of the references to colour in this figure legend, the reader is referred to the web version of this article.)

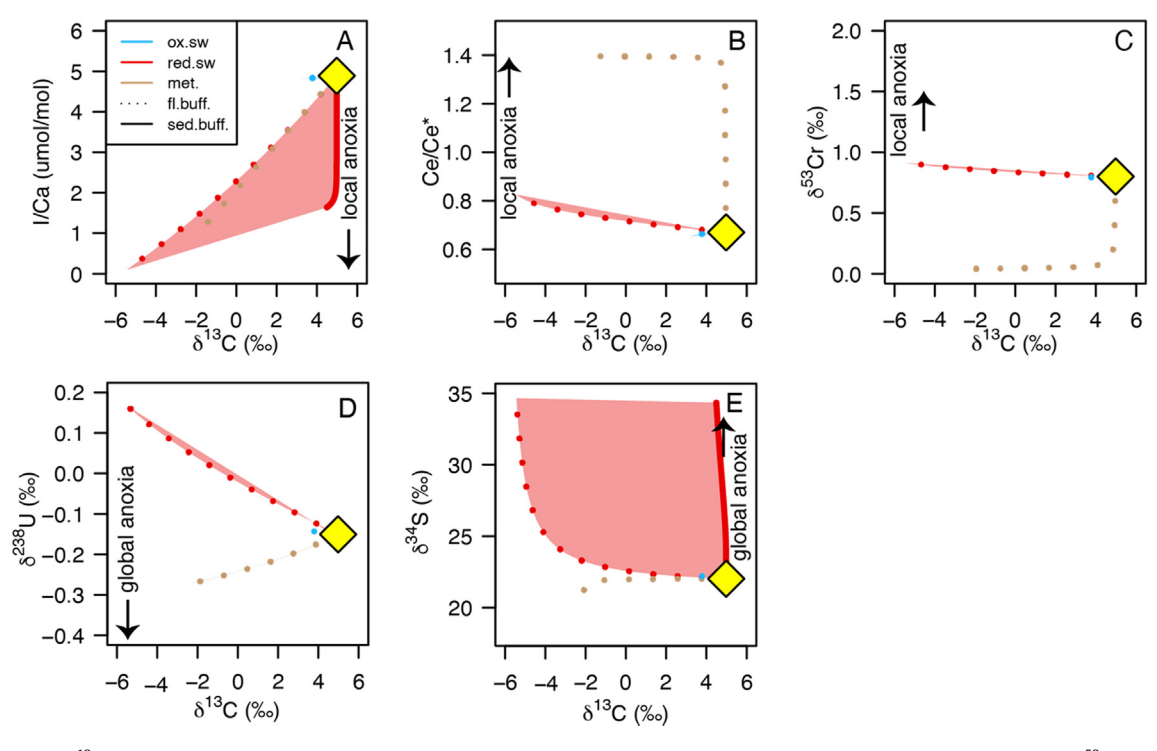


**Fig. 4.** Cross-plots of  $\delta^{13}$ C vs paleoredox proxies of diagenesis of primary aragonite from an initially oxic water column: (A) I/Ca, (B) Ce/Ce\*, (C)  $\delta^{53}$ Cr, (D)  $\delta^{238}$ U, (E)  $\delta^{34}$ S. Multiple valence states for Cr and U can be precipitated in calcite. The yellow diamond represents the starting composition. The lines represent fluid- (dotted line) and sediment-buffered (thick lines) conditions for meteoric (brown), oxidizing seawater (blue), and reducing seawater fluids (red). The arrows indicate the traditional proxy interpretation in the absence of diagenetic alteration. (For interpretation of the references to colour in this figure legend, the reader is referred to the web version of this article.)

# 5. Discussion

# 5.1. Sources of model uncertainty

Our endmember model parameterization is based on available experimental or observational constraints and considers a range of endmember fluid compositions, thus accounting for consider-

able natural variability while avoiding uncertainties in biogeochemical reaction constraints. The true uncertainty of these diagenetic alteration processes should include the full range of fluid geochemistry and diagenetic carbonate mineral parameters. Compared to some minor elements in carbonates, such as Sr or Mg (reviewed in Fantle et al., 2020), the full parameter range has not yet been explored for most redox-sensitive trace elements.

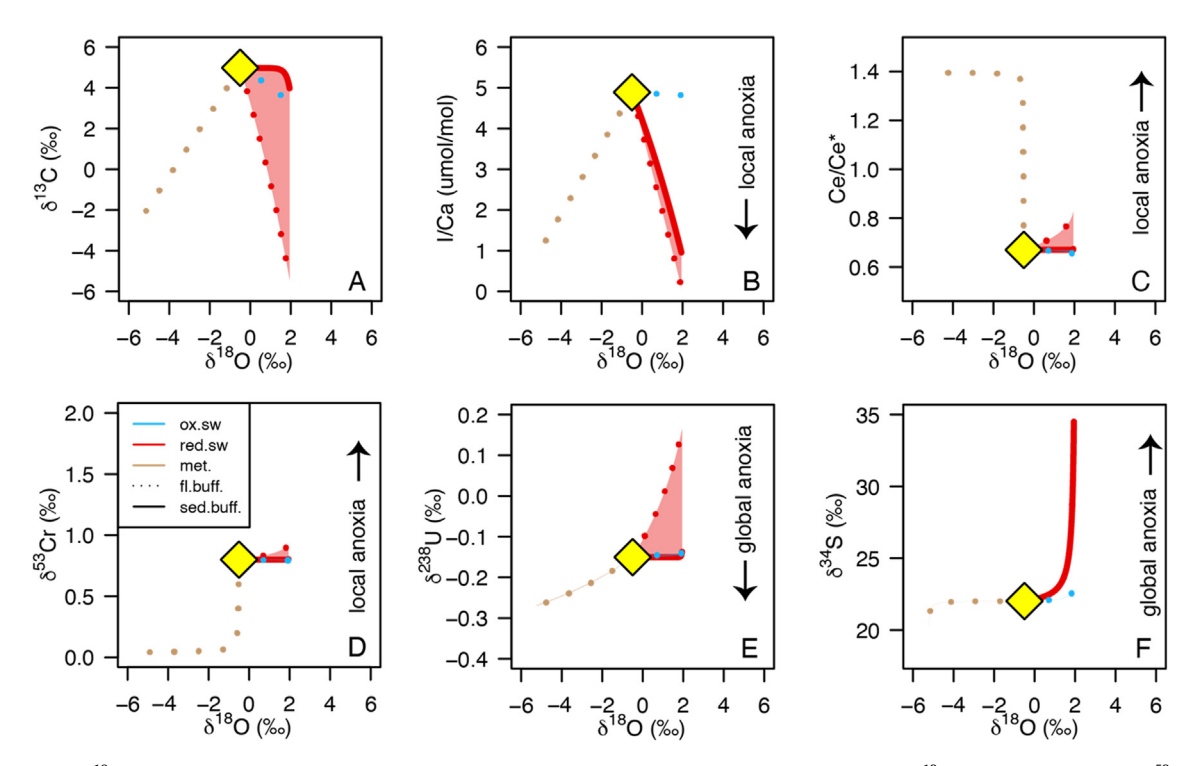


**Fig. 5.** Cross-plots of  $\delta^{18}$ O vs paleoredox proxies of diagenesis of primary aragonite from an initially oxic water column: (A)  $\delta^{13}$ C, (B) I/Ca, (C) Ce/Ce\*, (D)  $\delta^{23}$ Cr, (E)  $\delta^{238}$ U, (F)  $\delta^{34}$ S. Multiple valence states for Cr and U can be precipitated in calcite. The yellow diamond represents the starting composition. The lines represent fluid- (dotted lines) and sediment-buffered (thick lines) conditions for meteoric (brown), oxidizing seawater (blue), and reducing seawater (red) fluids. The arrows indicate the traditional proxy interpretation in the absence of diagenetic alteration. (For interpretation of the references to colour in this figure legend, the reader is referred to the web version of this article.)

Here, we highlight the key sources of uncertainty specific to redox proxies in carbonates (see <u>Supplementary Material</u> for further discussion). Additional research to address these knowledge gaps would improve diagenetic models and interpretations of carbonate geochemistry more broadly.

# 5.1.1. Constraints on proxy biogeochemical reactions

Our endmember fluid approach is broadly justified by its simplicity and thus wider applicability, the availability of constraints for endmember fluid geochemistry (see Table 2), the short diagenetic reaction length scales of I, U, Cr, and Ce reduction relative to that considered in the model (Figs. 1 & S1), and our overarching goal of comparing primary seawater geochemical retention in sediment- vs fluid-buffered conditions, as constrained via  $\delta^{44}$ Ca (Fig. 6). The similar outcomes of our endmember  $\delta^{34}$ S model comparison to the fixed-sulfate reduction rate model of Bryant et al. (2022) provides some justification for the applicability of both approaches (Fig. S4). A more comprehensive reaction network that more directly considers the biogeochemical evolution of proxies beyond S requires extensive experimental and field studies for parameterization and model-data calibration that are currently unavailable. To illustrate, only three studies have measured iodine speciation in marine porewaters (Kennedy and Elderfield, 1987a, b; Upstillgoddard and Elderfield, 1988), but no comparison to the I/Ca of carbonate sediment is available. Only one study has measured porewater U concentrations and isotopes during early carbonate diagenesis (Romaniello et al., 2013), but constraints on the U oxidation state in porewaters or the solid are unavailable. The only known study with constraints on pore fluid Ce/Ce\* during carbonate diagenesis comes from a methane seep (Himmler et al., 2010), which is not applicable to carbonate platforms. Further, to our knowledge, no study has analyzed porewater Cr concentrations, speciation, or isotopic composition evolution during carbonate diagenesis. Moreover, I, Cr, and U undergo rapid abiotic reduction in the presence of sulfide (Jia-Zhong and Whitfield, 1986; Pettine et al., 1994; Hua et al., 2006; Boonchayaanant et al., 2010). Given the presence of  $\mu$ M-levels of sulfide accumulation during very early diagenesis in carbonates (Romaniello et al., 2013), the sub- $\mu$ M concentrations of I, U, and Cr in seawater indicate that these elements will be rapidly reduced in marine pore fluids once highly reactive Fe has been titrated through precipitation of pyrite. Additional studies are necessary to understand the reduction kinetics of both microbial reduction during organic matter oxidation and abiotic reduction with sulfide, the isotope fractionations associated with biotic and abiotic reduction, and how to integrate redox sensitive systems in porewaters and sediments across diverse early diagenetic carbonate-rich environments.

# 5.1.2. Impacts of local Fe/Mn oxides on trace element geochemistry

Our model does not explicitly consider the delivery of trace elements sorbed to Fe/Mn oxides to local sediments, which can cause isotopic and concentration variations in carbonates unrelated to seawater chemistry. This is particularly true for Cr isotopes and Ce/Ce\* (Liu et al., 2019; Wang et al., 2021) and its importance remains uncertain for other proxies (e.g., Clarkson et al., 2020). We emphasize a multi-proxy approach, including variations in Mn concentrations, for recognizing such conditions, which are outlined in detail for individual proxies in these previous studies.

# 5.1.3. Trace element variability and behavior in meteoric fluids

Of the fluids considered in this modeling, the meteoric diagenetic scenario—specifically, how element incorporation varies with pH and ionic strength—is the most poorly constrained. Due to the absence of extensive datasets, if any, for all the elements of interest in meteoric fluids, particularly for the redox sensitive geochemical systems, we used average compositions of rivers or groundwaters.

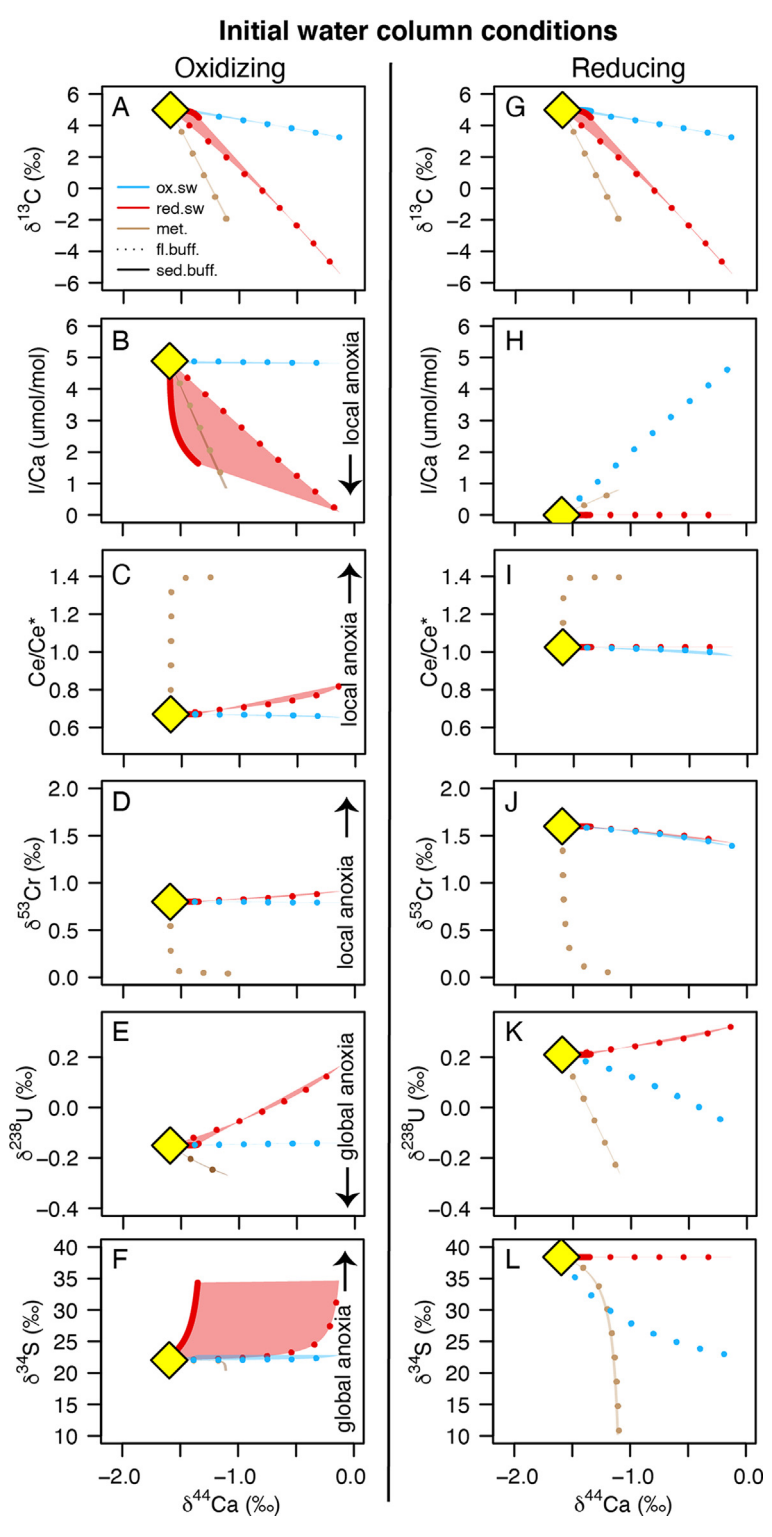


**Fig. 6.** Cross-plots of  $\delta^{44}$ Ca (reported relative to modern seawater) vs paleoredox proxies: (A)  $\delta^{13}$ C, (B) 1/Ca, (C)  $Ce/Ce^*$ , (D)  $\delta^{53}$ Cr, (E)  $\delta^{238}$ U, (F)  $\delta^{34}$ S, where the initial water-column redox state is oxidizing (left column) or reducing (G-L; right column). Multiple valence states for Cr and U can be precipitated in calcite. The yellow diamond represents the initial composition. The lines represent fluid- (dotted lines) and sediment-buffered (solid lines) conditions for meteoric (brown), oxidizing seawater (blue), and reducing seawater (red) fluids. The arrows indicate the traditional proxy interpretation in the absence of diagenetic alteration. (For interpretation of the references to colour in this figure legend, the reader is referred to the web version of this article.)

However, global compilations of river and groundwater geochemistry exhibit a remarkably large range on various spatial and temporal scales, varying with local climate, soils, and bedrock (e.g., McClain and Maher, 2016). The bedrock lithology impacting meteoric waters can have a large modulating effect: waters that have

mostly interacted with carbonates are likely to have geochemical compositions strongly influenced by carbonate geochemistry (e.g., waters that could be considered submarine groundwater; Holmden et al., 2012), whereas waters that have exchanged with siliciclastic rocks may be very different geochemically. Meteoric

fluids may also become reducing if sufficient organic matter is present in the carbonate sediment or in the aquifer. Such a scenario—which is outside the scope of this study—would impact the redox proxies independent of  $\delta^{18}$ O and other traditional markers for meteoric alteration.

5.1.4. Oxidation states of Cr and U incorporated in carbonate minerals Co-precipitation and isotope fractionation of Cr and U in calcite are expected to depend on which valence states of Cr and U are incorporated into the carbonate mineral. This can be a major source of uncertainty if the distribution of redox species in the mineral can vary (e.g., as a function of sedimentology). Although these factors have been discussed previously (e.g., Holmden et al., 2016; Clarkson et al., 2020; Zhang et al., 2020), targeted

mineral can vary (e.g., as a function of sedimentology). Although these factors have been discussed previously (e.g., Holmden et al., 2016; Clarkson et al., 2020; Zhang et al., 2020), targeted investigation of Cr and U redox variability in these settings and in this context are necessary to fully characterize the range of potential diagenetic trajectories. See Supplementary Material for further discussion and sensitivity analyses that consider Cr and U oxidation states.

#### 5.1.5. Redox-sensitive trace elements in dolomite

Calcite and dolomite are the two most dominant minerals in the carbonate rock record, and though they are nearly equally abundant in the Phanerozoic (Mackenzie and Morse, 1992), dolomite is the predominant carbonate mineral in the Precambrian (Cantine et al., 2020). The geochemistry of dolomite and of dolostones are already in widespread use for constructing ancient seawater chemistry, yet constraints on the fidelity of this archive to preserve primary seawater trends are lacking. The vast majority of previous laboratory studies that investigated trace element incorporation and isotope fractionation in carbonate minerals have focused on calcite rather than dolomite (reviewed in Smrzka et al., 2019). However, accurately modeling the expected alteration direction and pathways during dolomitization requires stronger experimental constraints on partition coefficients and isotope fractionation factors of redox-sensitive elements, in addition to ground-truthing these predictions in a range of dolomites (Hardisty et al., 2017; Herrmann et al., 2018; Zhang et al., 2018, 2019).

# 5.1.6. Data constraints from the same sample sets

Examples of  $\delta^{44}$ Ca and/or  $\delta^{26}$ Mg measured in the same sample sets as paleoredox proxies are rare (Bryant et al., 2022; the Permian-Triassic example discussed in Section 5.5), thus limiting model calibration against well-constrained observations and appropriate examples of ancient applications. Even the extensive diagenetic ( $\delta^{44}$ Ca and  $\delta^{26}$ Mg) and paleoredox proxy data sets from Clino and Unda cores (Section 5.3) were measured in different samples, limiting their potential as a calibration tool. Going forward, integrated studies should be prioritized to move forward important debates regarding the preservation of secular seawater vs diagenetic geochemical signatures during important intervals of Earth history.

# 5.2. Proxy resistance to diagenetic change based on water–rock model results

We can determine the relative order of proxy resistance to significant diagenetic change for each geochemical system and for each diagenetic scenario by determining the water–rock ratio at which the system has been 50% altered between the initial and final reset values (Fig. 2). We focus on the direction of change, rather than absolute values, because variations in primary seawater signatures through time relative to the modern can impact absolute values. Of the non-redox sensitive proxies,  $\delta^{18}{\rm O}$  and  $\delta^{26}{\rm Mg}$  can be reset with very little fluid interaction (i.e., lower

water–rock ratios) than Sr/Ca, with  $\delta^{13}$ C and  $\delta^{44}$ Ca reset at the highest water–rock ratios. Apart from  $\delta^{18}$ O, oxidizing and reducing seawater–derived fluids can reset geochemical values at lower water–rock ratios than meteoric fluids because concentrations are highly diluted (Table 2).

For the redox-sensitive proxies, CAS and  $\delta^{34}\mathrm{S}$  can be reset at the lowest water-rock ratios. The  $\delta^{53}\mathrm{Cr}$  system is altered with meteoric fluids at water-rock ratios between 10 and  $10^2$  but high water-rock ratios of  $\sim 10^4$  are predicted for 50% alteration under seawater-derived fluids. Meteoric and reducing seawater alteration of I/Ca ratios can occur at intermediate water-rock ratios (i.e., 10-100). Uranium concentrations and isotopes are most susceptible to alteration in meteoric environments and require higher water-rock ratios to alter when the diagenetic fluid is reducing, although the final change in  $\delta^{238}\mathrm{U}$  and [U] is also largest when altered with reducing seawater. The Ce/Ce\* anomaly appears to be the most robust, requiring the highest water-rock ratios to reach 50% alteration when the diagenetic fluid is reducing seawater.

### 5.3. Diagenetic model calibration against Bahamas data

To validate our use of the model from Ahm et al. (2018) for redox proxies, we use an existing geochemical dataset from the intensively studied Clino and Unda cores of the Great Bahama Bank that includes each of the modeled proxies of interest (Figs. 7, S9). Specifically, we hypothesize that the geochemistry of sediments from Clino and Unda represent mixing of carbonate minerals (aragonite/HMC, LMC, dolomite) that each reflect unaltered primary (aragonite/HMC) or diagenetic endmember geochemistry (LMC and dolomite) under different conditions (e.g., Figs. 4-6). This hypothesis is driven by previous  $\delta^{13}C_{carb}$  and  $\delta^{44}Ca$  studies of the Bahamas shelf-to-basin that observed variable CaCO<sub>3</sub> mineralogy across the transect that is correlated with  $\delta^{13}C_{carb}$  (Higgins et al., 2018; Swart and Eberli, 2005). We test this hypothesis by predicting the downcore geochemical trends for Clino and Unda using the quantified mineral contributions of aragonite/HMC, LMC, and dolomite, combined with primary and endmember diagenetic geochemistry used in and outputted from our diagenetic model simulations. Importantly, our model parameters for the redox proxies were largely chosen independent of Clino and Unda (Table 2) with the intention of performing a model-data comparison with these well-constrained cores.

The geochemistry and sedimentology of the Clino and Unda cores are among the best characterized in Earth history from a carbonate setting. These cores capture a series of proto-carbonate platforms which prograded from the Miocene to Neogene (Kenter et al., 2001). The Clino core contains slope deposits which transition upward to a platform consisting of reefal and sand deposits. The Unda core alternates between deeper marginal deposits and shallow-water platform sands and reefal deposits (Swart and Melim, 2000). In each case, these successions and transitions are tied to sea-level change which drove variations in exposure to meteoric fluids and the relative proportion of platform-derived aragonite and open-ocean derived calcite (Droxler et al., 1983; Droxler and Schlager, 1985; Schlager et al., 1994; Swart and Eberli, 2005). Therefore, this calibration also captures the outcome of mixing of these different carbonate sources and their expected geochemical and diagenetic compositions. Previous studies have constrained the upper 150 m of Clino and 110 m of Unda as having experienced repeated interaction with meteoric fluids (Swart and Oehlert, 2018) identified by multiple horizons containing caliche layers and other sedimentological evidence for subaerial exposure. In addition, these meteoric zones are characterized by nearquantitative diagenetic conversion of primary aragonite to LMC as well as negative  $\delta^{13}C_{carb}$  values typical of subaerial diagenesis

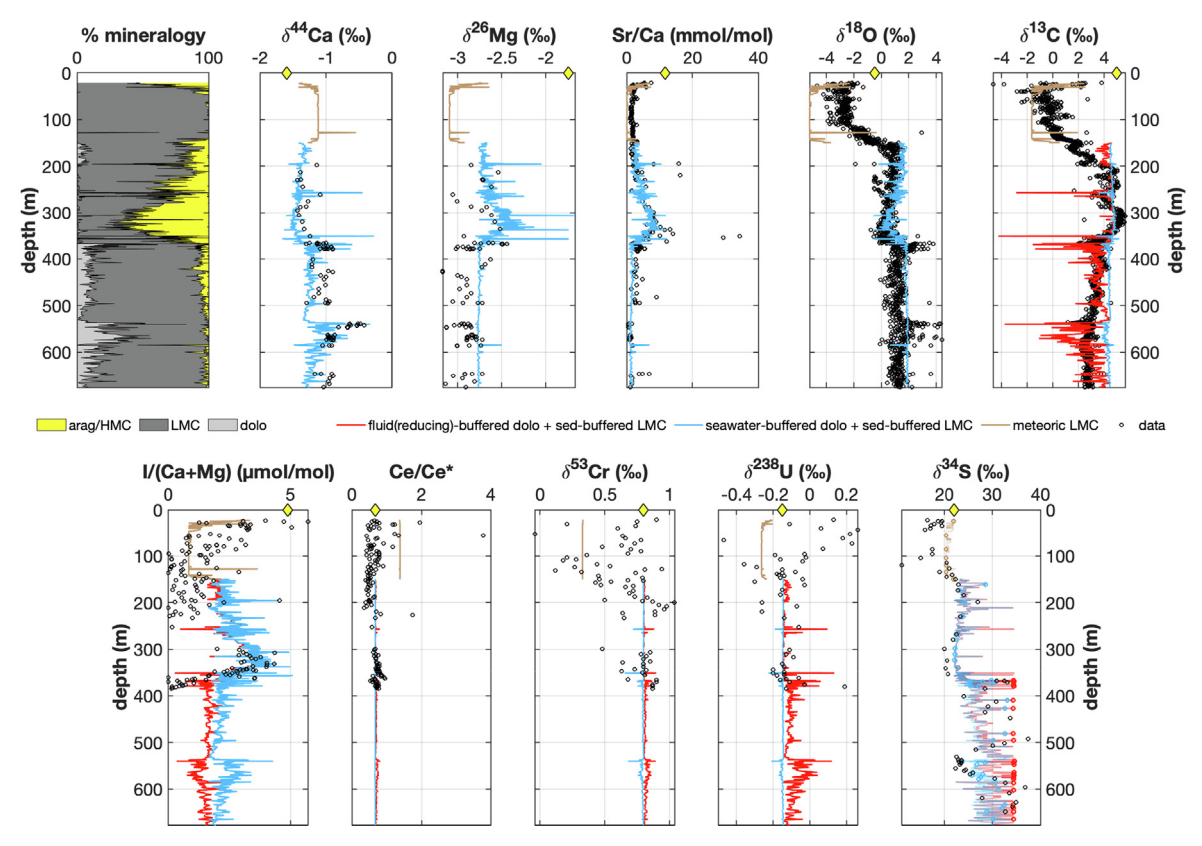


Fig. 7. Clino core mineralogy and geochemical data. The mineralogy of this core was predominantly aragonite and deposition occurred under an oxic water-column. Sediments were subsequently recrystallized to low-Mg calcite or dolomitized. The yellow diamonds mark the initial geochemical compositions used in our model. Data are shown for  $\delta^{13}C_{\text{carb}}$  and  $\delta^{18}O$  (Melim et al., 1995; Oehlert and Swart, 2014; Stewart et al., 2015; Hardisty et al., 2017; Higgins et al., 2018), mineralogy (Melim et al., 1995; Hardisty et al., 2017; Murray et al., 2021),  $\delta^{34}C$  (Ca + Mg) (Hardisty et al., 2017),  $\delta^{238}U$  (Chen et al., 2018),  $Ce/Ce^*(Liu \text{ et al.}, 2019)$ ,  $\delta^{34}C$  (Murray et al., 2021),  $\delta^{35}Cr$  (Wang et al., 2021),  $\delta^{44}Ca$  and  $\delta^{24}Mg$  (Higgins et al., 2018). The blue, red, and brown circles in the  $\delta^{34}S$  plot reflect modeled values based on the mineralogy of the samples from Murray et al. (2021), the source of the  $\delta^{34}S$  data. The red and blue lines are both modeled, but overlap for  $\delta^{44}Ca$ ,  $\delta^{24}Mg$ ,  $\delta^{18}O$ , and Sr/Ca, since they are not redox-sensitive. (For interpretation of the references to colour in this figure legend, the reader is referred to the web version of this article.)

within developing soils (Melim, 1996; Gill et al., 2008). Below this meteoric zone, the sediments have undergone diagenesis exclusively in marine pore fluids (Melim et al., 2004; Swart and Oehlert, 2018).

The mixing model equations and detailed justification for key assumptions are described in detail in the Supplementary Material and are briefly outlined here: (1) Aragonite and HMC are primary bank-derived minerals precipitated from an oxidizing water column. (2) Aragonite and HMC have identical initial geochemistry and behave similarly during diagenesis. (3) LMC is a diagenetic mineral. (4) LMC from the meteoric zones—the upper 150 m of Clino and 110 m of Unda—is derived from aragonite-to-calcite recrystallization with oxidizing meteoric diagenetic fluids. (5) Below the meteoric zones, LMC is derived from aragonite-to-calcite recrystallization under sediment-buffered conditions with reducing pore fluids. (6) Dolomite is a diagenetic mineral formed under fluid-buffered conditions. (7) Fluid-buffered dolomite has the endmember geochemistry of fluid-buffered LMC, but whether the fluid was oxidizing or reducing is not known.

Based on these assumptions and the mineralogy of Clino, the predicted geochemistry of this core is presented in Fig. 7. The Unda core is also modeled (Fig. S9), but because of more limited geochemical data and abundant dolomite (which is not explicitly considered in the model), the results are described in the Supplementary Discussion. Given the extensive assumptions required for the diagenetic and mixing models, the simulated results show a qualitative overlap with the observations (Figs. 7 and S9). In addition to providing a proof-of-concept for the model,

this exercise also supports the underlying hypothesis of the mixing model: i.e., that primary aragonite was derived from an oxidizing water column and the final sediment geochemistry is dictated by the diagenetic regime under a range of fluid- and sediment-buffered conditions with variable fluid redox states.

We suggest that the most important takeaway from the modeldata comparison for the meteoric zone of Clino (modeled in brown; Fig. 7) is the potential for paleoredox proxies to undergo significant deviations from seawater values from meteoric diagenesis (Hardisty et al., 2017; Chen et al., 2018; Wang et al., 2021). As most clearly distinguished via  $\delta^{18}O$  (Fig. 5), the model results for paleoredox proxies match the directionality of downcore trends for  $\delta^{13}$ C, I/Ca, Ce/Ce\*, and  $\delta^{34}$ S but do not match the wide range of the observations in Clino (Fig. 7). The comparatively broader observational range relative to the model results further bolsters our conclusion that, apart from  $\delta^{34}$ S (McClain et al., 1992), trace element concentrations and isotopic compositions of meteoric fluids of carbonate platforms, as well as the  $K_D$  values of trace element incorporation into LMC under these geochemical conditions, are undercharacterized and contribute significant uncertainty to our model and interpretations of the paleoredox proxies in meteoric waters.

Below the meteoric zone of Clino (150–350 mbsf; Fig. 7), qualitative agreement between the modeled and observational data for the redox-sensitive proxies, including  $\delta^{13}$ C, supports our assumption that non-meteoric LMC from these cores was formed during mostly reducing, sediment-buffered alteration. Most of this interval consists of aragonite and LMC, and our model predictions, derived by assuming that the aragonite endmember reflects unal-

tered values and that the LMC endmember reflects sedimentbuffered alteration, largely mimics the bulk carbonate geochemistry. For  $\delta^{34}$ S, samples with even minor aragonite tend to preserve modern seawater  $\delta^{34}$ S values because of the high CAS concentration in aragonite compared to diagenetic, sediment-buffered LMC (3,766 vs 147 ppm). However, below 350 mbsf, the  $\delta^{34}$ S record consists of largely aragonite-free samples relative to the background and thus tends to track diagenetic processes (Murray et al., 2021). Because the intervals sampled for  $\delta^{34}$ S targeted lowaragonite intervals, we focus on the mixing model results derived using the mineralogy of the same samples from Murray et al. (2021) to compare with the  $\delta^{34}$ S data (red and blue circles in Figs. 7 and S9; n = 42 Clino and 12 Unda samples). Given this consideration, the  $\delta^{34}$ S record below 350 mbsf in Clino provides additional constraints on sediment-buffered LMC, as these results indicate that higher  $\delta^{34}$ S values correspond to a greater proportion of LMC. Although the model results broadly mimic the trends downcore, they do not reproduce the high  $\delta^{34}$ S values observed in some intervals (Fig. 7). This suggests that the parameterization for sulfur isotope fractionation (Table 2) does not adequately capture the full range possible during sulfate reduction or other processes impacting  $\delta^{34}$ S heterogeneity (e.g., Present et al., 2015, 2019; Murray et al., 2021).

In the dolomitized zones of Clino and Unda (e.g., 500–600 mbsf in Clino and below 100 mbsf in Unda), there is good model-data agreement for  $\delta^{13}$ C,  $\delta^{34}$ S, and Ce/Ce\*. This ultimately supports dolomitization as a process that can preserve  $\delta^{13}$ C during seawater-buffered diagenesis and hence aid in recognizing similar conditions in the geologic record (Ahm et al., 2018, 2019, 2021; Bold et al., 2020; Jones et al., 2020; Crockford et al., 2021; Nelson et al., 2021). Conversely, we note that the intervals with minor dolomite—termed "background" dolomite in Swart et al. (2001)—show a better model fit for  $\delta^{13}$ C and  $\delta^{34}$ S when the diagenetic fluid is reducing (red) than when it is oxidizing (blue), consistent with previous interpretations that these dolomites formed in fluids more reducing than, and relatively isolated from, seawater (Swart and Melim, 2000).

In summary, despite uncertainties arising from meteoric diagenesis and the potential for multiple diagenetic events, our model has the potential to simulate broadly natural diagenetic alteration if the proper mineralogical and sedimentological context are considered. These results also highlight the potential for a combination of diagenetic scenarios, impacting the same strata, to result in large stratigraphic variability in these geochemical proxies—which suggests that proxy records in Earth's history may exhibit shifts and scatter unrelated to secular seawater change.

# 5.4. Model insights into applying and interpreting carbonate paleoredox proxies

A powerful application of diagenetic models is the potential to leverage the predicted relative sensitivity of multiple individual proxies to diagenetic resetting (and other conditions) to identify the diagenetic conditions that can best preserve the primary seawater geochemical signatures for an individual proxy (Ahm et al., 2018, 2019, 2021; Bold et al., 2020; Jones et al., 2020; Crockford et al., 2021; Nelson et al., 2021; Bryant et al., 2022). These conditions of ideal preservation can vary for the paleoredox proxies in this study.

Unsurprisingly, our analysis indicates that the redox state of the diagenetic fluid is an essential constraint for each of the paleoredox proxies: i.e., reducing vs oxidizing diagenetic fluids result in different endmember diagenetic calcite compositions under fluid- and sediment-buffered conditions. Analogous results were found for carbonate  $\delta^{13}$ C for fluid  $\delta^{13}$ C and DIC endmembers chosen to represent progressive organic matter oxidation in porewaters (Fig. S7;

Derry, 2010; Ahm et al., 2018). We find that seawater-derived, fluid-buffered alterations, where the redox state of the pore fluids matches that of the water column (i.e., seawater-buffered), represent the best-case-scenario for all proxies of interest. Importantly, seawater-buffered diagenesis preserves water column geochemistry regardless of whether the water column is reducing or oxidizing (Fig. 6). Sediment-buffered diagenesis, when the pore fluid has the same redox conditions as the overlying water column, is also predicted to result in little-to-no alteration of the paleoredox proxies (Fig. S1). This scenario is likely most commonly manifested in initially reducing water column regimes, meaning these have amongst the highest potential to preserve primary seawater chemistry. However, matching of water column and pore fluid redox conditions is unlikely for oxidizing water columns in shallow marine carbonate settings where anaerobic respiration can occur within the upper 10's of cm (e.g., Romaniello et al., 2013). An exception may be for proxies less sensitive to reducing conditions (i.e., at lower Eh thresholds) in slope and pelagic carbonate settings. For example, this may be relevant for  $\delta^{34}$ S because sulfate reduction can be located deeper in the sediment column (~50-350 m; Kramer et al., 2000).

An effective approach for discerning between oxidizing and reducing seawater-buffered conditions is plotting paired  $\delta^{44}$ Ca and paleoredox proxy data and determining the relationship between fluid- and sediment-buffered endmembers. In this way, the directionality of the slopes between endmembers, as well as the field between the endmembers and the original composition-like that shown in Fig. 6-can be used to approximate the samples most likely to represent a given diagenetic scenario. Most specifically, application of Ce/Ce\* and, perhaps  $\delta^{238}$ U, alongside  $\delta^{44}$ Ca has the most potential to identify diagenesis under seawater-buffered conditions. For these proxies, samples exhibiting a fluid-to-sediment-buffered spectrum of  $\delta^{44}$ Ca values, but limited variability in  $\delta^{238}$ U and Ce/Ce\*, can be used to constrain the fluid-buffered endmember as being seawater buffered. These identified "seawater-buffered" sample sets may then be those best used for other paleoredox proxies of interest.

Our model predicts that  $\delta^{238}$ U and Ce/Ce\* primary proxy values are altered by <10% from typical modern carbonate values under both sediment-buffered conditions and seawater-buffered diagenetic conditions (Figs. 3 and 6). Alteration of <10% is likely to have little impact on proxy interpretation of Ce/Ce\* because ratios near the anoxic-oxic threshold are typically categorized as ambiguous (e.g., Tostevin et al., 2016). Ce/Ce\* applications are also supported by comparison with the Clino and Unda data: Ce/Ce\* appears to be most robust and is relatively invariant with depth (Figs. 7 and S9). Alteration of < 10% is also unimportant for  $\delta^{238}$ U because it is within the range of typical analytical uncertainty (0.05%) and stratigraphic variability (e.g., Chen et al., 2018; Tissot et al., 2018). However, as was observed for  $\delta^{53}$ Cr, variable  $\delta^{238}$ U in Clino and Unda clearly indicate effects of dolomitization and other processes (such as incorporation of multiple valence states) that lack adequate calibration in our model and therefore we suggest further research is needed to understand the fidelity of  $\delta^{53}$ Cr and  $\delta^{238}$ U (see Fig. S8).

An alternative or complementary approach for identifying primary seawater geochemical signatures is to exploit the high sensitivity of I/Ca to diagenesis if primary aragonite from an oxidizing water column is altered in reducing fluids of any kind (Hardisty et al., 2017). Specifically, the only diagenetic scenario that preserves elevated primary I/Ca values in diagenetic calcite is seawater-derived, oxidizing fluid-buffered diagenesis (Fig. 6). This is because I/Ca tracks ambient IO<sub>3</sub><sup>-</sup> that is reduced during overlapping iodinous/nitrogenous early diagenetic conditions directly after or even overlapping with oxic respiration (Fig. 1). In addition to a high sensitivity to more reducing conditions, I/Ca is also a

concentration-based proxy, which further increases its likelihood of being overprinted as conditions evolve toward sediment-buffered diagenesis or low water–rock ratios. In this way, if it can be demonstrated that I/Ca ratios are preserving primary oxidizing, seawater-like geochemistry (i.e., maintains high values) then one can have the highest confidence that  $\delta^{53}$ Cr, Ce/Ce\*,  $\delta^{238}$ U, and  $\delta^{34}$ S could as well.

While this approach is powerful, we note that it is limited in scope. First, the application of I/Ca or other proxies for diagenetic screening of fluid redox conditions may be overly conservative in some cases. Specifically, fluids that are reducing with respect to  $IO_3^-$  need not be reducing with respect to these other proxies, so it is possible to alter I/Ca ratios while the diagenetic fluid remains oxidizing with respect to other proxies. For example, this is a potential scenario for the dolomitic intervals of Clino and Unda. Secondly, low I/Ca ratios are ambiguous and could represent iodinous conditions, multiple types of diagenetic overprinting, or seawater-buffered diagenesis that preserves primary aragonite geochemistry from a reducing water column (Fig. 6). Therefore, low I/Ca ratios do not exclusively indicate diagenesis, but instead require additional constraints to distinguish between these scenarios.

In sum, this study highlights that the combination of datamodel comparison and mineralogical and stratigraphic context has the potential to improve our understanding of the evolution of carbonate mineralogy and diagenesis through Earth history, in addition to identifying secular seawater chemical evolution. Specifically, the combination of the sensitivity of the paleoredox proxies to seawater-buffered diagenesis and their respective redox thresholds, and hence early burial conditions, alongside the broader sensitivity of  $\delta^{44}$ Ca to fluid- vs sediment-buffered conditions (e.g., Fig. S1), further refines our ability to characterize ancient diagenetic environments. This is akin to applications of Fe speciation in shales to identify the presence of Fe- vs sulfidedominated diagenetic fluids (Hardisty et al., 2018), but further extending this to identifying seawater-buffered conditions (see Fig. 1). For example, iodinous pore fluids can be identified with the existing record: while I/Ca is low through most of Earth history (e.g., Lu et al., 2020), there are LMC- and dolomite-derived values elevated above that expected from diagenesis extending into the Proterozoic. This suggests that, while perhaps not pervasive in Clino, seawater-buffered diagenetic environments could be relatively common and hence their recognition may provide insights into carbonate mineralogical evolution. A specific example includes the potential to combine Ca-Mg isotopes and paleoredox proxies to identify trends in so-called early dolomitization-i.e., the dolomite problem—which has been hypothesized from fabric retentive vs destructive dolomite and some geochemical evidence, but remains under debate (Tucker, 1982; Hardisty et al., 2017). Further, we emphasize that stratigraphic context plays an important role in recognizing seawater-buffered environments alongside modeling results (e.g., Nelson et al., 2021). Lastly, as is outlined in the following section, our models are inherently local and therefore do not consider globally observed patterns in multiple proxies, which should be considered as an additional criterion in any carbonate proxy applications.

# 5.5. Revisiting carbonate paleoproxy records through Earth history: lessons from the Permian-Triassic

Identifying primary geochemical composition by comparing paleoredox proxies does not account for the potential for evolving seawater chemistry across constant or changing diagenetic conditions. Coeval trace element- $\delta^{44}$ Ca stratigraphic trends have been suggested to be difficult to interpret in the context of secular seawater evolution and are instead commonly used as a litmus test for

identifying potential diagenetic overprints (Husson et al., 2015). Importantly, the Late Permian to Middle-Late Triassic exhibits stratigraphic trends in  $\delta^{44}\mathrm{Ca}$ ,  $\delta^{13}\mathrm{C}$ ,  $\delta^{18}\mathrm{O}$ , and  $\delta^{238}\mathrm{U}$ , with previously published data analyzed on the same samples (Payne et al., 2007, 2010; Lau et al., 2016, 2017; Silva-Tamayo et al., 2018), which enables us to apply our modeling framework to distinguish between secular seawater change and interpretations of diagenetic alteration. At the same time, the end-Permian extinction (ca. 252 Ma) and its aftermath is a time interval when global carbon cycle perturbations and marine redox changes have been independently corroborated through paleontology, lithological and sedimentological changes, modeling predictions, organic geochemical proxies and biomarkers.

The geochemical shifts that mark the Permian/Triassic boundary are most parsimoniously interpreted as secular changes in seawater, and although diagenetic alteration was certainly present and likely includes burial diagenesis, the geochemical trends cannot be explained by the early diagenetic model. Fig. 8 depicts the available data plotted on the relevant  $\delta^{44}$ Ca cross-plots from Fig. 6. This compilation includes two stratigraphic sections on opposite margins of the Paleo-Tethys ocean: Dajiang (Great Bank of Guizhou, South China) and Taşkent (Turkey). For simplicity, the data are binned into time intervals (defined in Fig. 8) and the values in each bin are then averaged if data are sufficiently available (i.e., n > 1). The discussion that follows is limited by the small number of samples for some of the time bins. We note that the initial modeled values of some proxies (i.e.,  $\delta^{13}$ C,  $\delta^{18}$ O) do not significantly overlap with the data because seawater  $\delta^{13}$ C and  $\delta^{18}$ O were different from the modern and because  $\delta^{18}$ O can reflect late-stage diagenetic processes not represented in our early diagenetic model; therefore, we focus this discussion on the predicted direction of change from diagenesis.

Here, we discuss the geochemical shifts during the main extinction interval (bins 1 to 3); the rest of the record is discussed in the Supplementary Materials. At Taşkent, the pre-extinction to main excursion record (Fig. 8, bins 1 to 2) exhibits a shift to lower mean values for  $\delta^{13}$ C,  $\delta^{44}$ Ca,  $\delta^{238}$ U, and  $\delta^{18}$ O, and no change in Ce/Ce\*. Such correlated shifts cannot be explained by a diagenetic scenario only (i.e., without a concomitant change in seawater chemistry). Specifically, correlated negative  $\delta^{13}$ C and  $\delta^{44}$ Ca shifts are only possible from a switch from seawater-buffered to meteoric diagenesis (Fig. 8A). This is consistent with negative shifts in  $\delta^{238}$ U and  $\delta^{18}$ O (Fig. 8B and 8D) but is not consistent with the insignificant difference in Ce/Ce\* (Fig. 8C) nor with sedimentological observations (e.g., Payne et al., 2007). Similarly, the shift to lower mean  $\delta^{238}$ U and  $\delta^{44}$ Ca values aligns with the prediction for diagenesis with reducing seawater (Fig. 8D), but this interpretation is inconsistent with the Ce/Ce\* and  $\delta^{13}$ C trends. These negative shifts are replicated at Dajiang for the same proxies, even though average  $\delta^{44}$ Ca is higher (-1.7 % $_{o}$  vs -1.4 % $_{o}$ ).

The next stratigraphic shift, from the main excursion to end of the Induan (Fig. 8, bins 2-3), is again inconsistent with solely a diagenetic driver. At Taşkent, average  $\delta^{13}$ C and  $\delta^{44}$ Ca values both increase—a relationship that is not predicted under any reasonable diagenetic scenario in the absence of a change in seawater  $\delta^{13}$ C. A shift to higher average  $\delta^{44}$ Ca and a small increase in  $\delta^{238}$ U is compatible with oxidizing seawater-buffered diagenesis (Fig. 8B-D), but the most parsimonious interpretation is a partial recovery to pre-perturbation environmental conditions, consistent with greater biodiversity of some taxa by the end of the Induan (Chen and Benton, 2012). At Dajiang, the changes in average  $\delta^{13}$ C,  $\delta^{44}$ Ca,  $\delta^{18}$ O, or  $\delta^{238}$ U are smaller but in the same direction as at Taşkent. Thus, key geochemical shifts in these records do not agree with predictions based on the early diagenetic model (and assumptions therein), bolstering interpretations of primary, rather than diagenetic, processes—which is independently supported by other

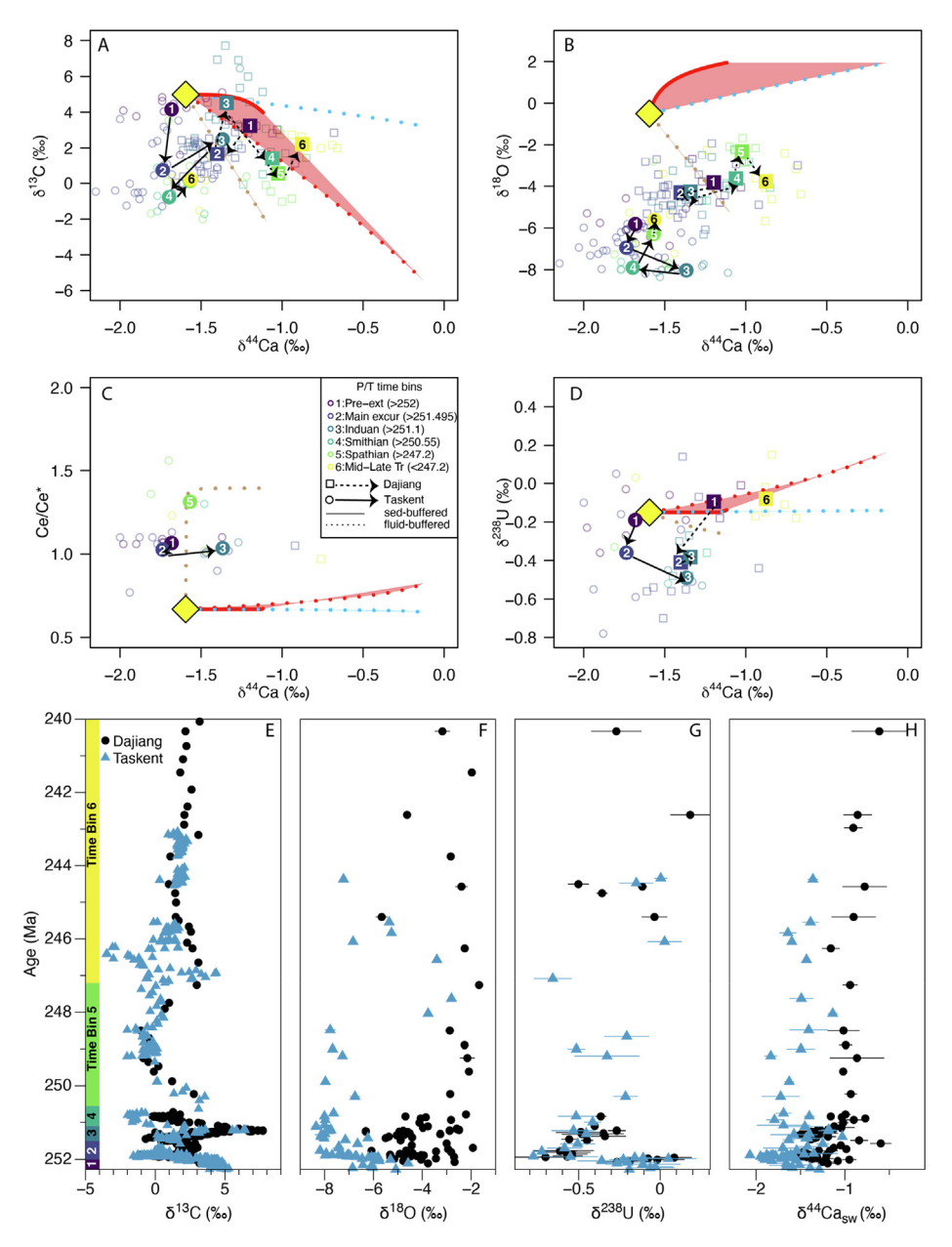


**Fig. 8.** Evaluation of paleoredox proxy data across a major biogeochemical perturbation. (A–D) Data from the latest Permian, Early Triassic, and Middle-Late Triassic are binned based on intervals with recognized perturbations and by sampling frequency, with circles for Taşkent, Turkey and squares for Dajiang, South China. Data were collected from the same sample and, except for Ce/Ce\*, were previously published (Payne et al., 2004, 2010; Lau et al., 2016, 2017; Silva-Tamayo et al., 2018). Methods for Ce/Ce\* are described in Lau et al. (2016). Large symbols represent the average values for each bin and are shown if n > 1. Arrows represent shifts from older to younger time bins if more than one paired sample was available. (E–H) Stratigraphic trends in  $\delta^{13}$ C,  $\delta^{18}$ O,  $\delta^{238}$ U, and  $\delta^{44}$ Ca. Ce/Ce\* are not shown due to the limited sample set. We do not include Dajiang  $\delta^{34}$ Ca data from (Wang et al., 2019) because no redox proxies were measured. Similarly, we do not include Dajiang  $\delta^{34}$ Ca was not analyzed in the same samples. P/T = Permian/Triassic; Pre-ext = Pre-extinction; Main excur = Main  $\delta^{13}$ C excursion; Mid-Late Tr = Middle-Late Triassic.

geologic evidence including the absence of meteoric cements. Instead of an early diagenetic explanation, these changes across the Permian/Triassic boundary are broadly consistent with a perturbation to the carbon cycle, replicated across multiple carbonate sections as well as marine and terrestrial organic carbon records (Payne et al., 2004; Horacek et al., 2007; Meyer et al., 2013; Cui et al., 2017), higher sea-surface temperatures reconstructed from  $\delta^{18}$ O of conodont apatite (Joachimski et al., 2012, 2020; Schobben et al., 2014), and expansive seafloor anoxia (e.g., Hülse et al., 2021). A similar data-model comparison can be conducted for other redox proxy datasets through Earth history to determine whether early diagenesis could be the primary driver of a geo-

chemical record or if other factors are likely applicable (such as secular seawater change, diagenetic processes, a change in contribution of different CaCO<sub>3</sub> polymorphs, etc.).

Though our models predict that seawater-buffered conditions (blue model lines) may be the best-case-scenario for retention of primary seawater values for all the paleoredox proxies, including  $\delta^{13}$ C, a range of fluid- to sediment-buffered  $\delta^{44}$ Ca values do not always imply paleoredox proxies (such as  $\delta^{238}$ U in this example) cannot record secular seawater change. Interpreted from a diagenetic perspective only, the higher  $\delta^{44}$ Ca at Dajiang (squares) compared to Taşkent (circles) could suggest that the Dajiang carbonates experienced greater fluid-buffered diagenesis and are

less likely to preserve seawater  $\delta^{44}$ Ca values whereas Taşkent carbonates experienced sediment-buffered diagenesis and are more likely to preserve seawater  $\delta^{44}$ Ca. Importantly, the  $\delta^{238}$ U records are comparable between sections (Fig. 8). As discussed in Section 5.4, the retention of  $\delta^{238}$ U signals across a sediment-to fluidbuffered gradient in  $\delta^{44}$ Ca provides evidence for seawater  $\delta^{238}$ U values in both sections and specifically that seawater-buffered conditions are likely in the fluid-buffered interval of Dajiang. Seawater-buffered conditions imply that the Dajiang carbonates might be best suited for applications of the broader paleoredox proxy suite, including  $\delta^{13}$ C. Despite the large observed range of  $\delta^{44}$ Ca values, the retention of seawater chemistry signals can also include changes in seawater  $\delta^{44}$ Ca itself that reflect mass imbalances, different proportions of CaCO<sub>3</sub> polymorphs, and changes in carbonate precipitation rate (Komar and Zeebe, 2016; Silva-Tamayo et al., 2018; Wang et al., 2019).

## 6. Conclusions

This study uses an increasingly popular diagenetic model framework (Ahm et al., 2018) for calcium and carbon isotopes to include a suite of paleoredox proxies—iodine ratios (I/Ca), the cerium anomaly (Ce/Ce\*), and carbonate-associated Cr, U, and S isotopes. Specifically, we model the recrystallization of aragonite sourced from both oxidizing and reducing water columns to low-Mg calcite with various diagenetic fluids (oxidizing seawater, reducing seawater, and meteoric fluids) and under conditions that are increasingly rock-buffered (fluid- to sediment-buffered). Like previous applications of  $\delta^{13}$ C and  $\delta^{44}$ Ca, our results indicate that the relative degree of fluid-buffering impacts the potential for a given proxy to preserve primary seawater chemistry following variable styles of diagenesis. Moreover, the consideration of the redox state of the fluid is demonstrated to be an additionally important constraint.

Ultimately, our model results quantitatively demonstrate that seawater-buffered conditions—or fluid-buffered conditions where the redox state of the diagenetic fluid is analogous to the seawater from which the primary aragonite precipitated—best preserve primary paleoredox signatures, including for  $\delta^{13}$ C. Importantly, fluidbuffered alterations with evolving redox conditions and progressive organic matter oxidation during early diagenesis-which will impact trace element speciation and isotope compositions as well as the  $\delta^{13}$ C of dissolved inorganic carbon—have high potential to alter the original geochemical composition of carbonates, and thus must be screened. The variable preservation potential of the paleoredox proxies can be leveraged to recognize seawater-buffered conditions. Ultimately, Ce/Ce\* and potentially  $\delta^{238}$ U are the most robust to diagenetic alteration whereas the extreme sensitivity of I/Ca to diagenetic overprinting, always to lower values, implies that elevated I/Ca uniquely indicates seawater buffered or primary mineral preservation.

Our model is calibrated and discussed in the context of case studies with Neogene Bahamas cores with well constrained diagenetic alterations (Clino and Unda) and the Permian/Triassic, both which have been measured previously for paleoredox proxies and calcium and carbon isotopes. Importantly, our Clino and Unda mixing model (Section 5.3) and the Permian/Triassic case study (Section 5.5) emphasize that simplified proxy-proxy model interpretations of complex geochemical data sets have the potential to mask important stratigraphic and mineralogical information and thus must be used with caution. However, when this context is considered, diagenetic and primary seawater geochemistry can potentially be determined. Going forward we recommend multiple steps necessary to improve the application of these and similar diagenetic models to paleoredox applications, including: additional

case studies comparing  $\delta^{44}$ Ca and paleoredox proxy data; field-based characterization of the concentrations and isotope compositions of redox-sensitive trace elements in meteoric fluids from carbonate platforms, which are essentially uncharacterized; experimental quantification of the potential for multiple redox states of the same element—most prominently for Cr and U—into carbonate minerals and their associated partition coefficients; and experimental quantification of partition coefficients for each of the paleoredox proxies into dolomite minerals, which are essentially unknown despite their widespread application to dolomite.

### **Data availability**

A link to the code is provided in "Research Data"

## **Declaration of Competing Interest**

The authors declare that they have no known competing financial interests or personal relationships that could have appeared to influence the work reported in this paper.

### Acknowledgements

D.S.H. acknowledges support from NSF-OCE 1829406. K.V.L. acknowledges support from NSF-SGP 2124802 and NSF-FRES 2021324. The authors thank Mohammed Hashim for early feedback on this study. We thank three anonymous reviewers and Associate Editor Chao Li for constructive comments that greatly improved this work.

#### Research data

Model code can be accessed at https://doi.org/10.2627/wrdz-sz05.

# Appendix A. Supplementary material

Supplementary material to this article can be found online at https://doi.org/10.1016/j.gca.2022.09.021.

# References

- Ahm, A.-S.-C., Bjerrum, C.J., Blättler, C.L., Swart, P.K., Higgins, J.A., 2018. Quantifying early marine diagenesis in shallow-water carbonate sediments. Geochim. Cosmochim. Acta 236, 140–159.
- Ahm, A.S.C., Bjerrum, C.J., Hoffman, P.F., Macdonald, F.A., Maloof, A.C., Rose, C.V., Strauss, J.V., Higgins, J.A., 2021. The Ca and Mg isotope record of the Cryogenian Trezona carbon isotope excursion. Earth Planet. Sci. Lett. 568.
- Ahm, A.-S., Husson, J., 2021. Local and global controls on carbon isotope chemostratigraphy. Cambridge University Press.
- Ahm, A.S.C., Maloof, A.C., Macdonald, F.A., Hoffman, P.F., Bjerrum, C.J., Bold, U., Rose, C.V., Strauss, J.V., Higgins, J.A., 2019. An early diagenetic deglacial origin for basal Ediacaran "cap dolostones". Earth Planet. Sci. Lett. 506, 292–307.
- Algeo, T.J., Li, C., 2020. Redox classification and calibration of redox thresholds in sedimentary systems. Geochim. Cosmochim. Acta 287, 8–26.
- Banner, J.L., 1995. Application of the trace element and isotope geochemistry of strontium to studies of carbonate diagenesis. Sedimentology 42, 805–824.
- Banner, J.L., Hanson, G.N., 1990. Calculation of simultaneous isotopic and traceelement variations during water-rock interaction with applications to carbonate diagenesis. Geochim. Cosmochim. Acta 54, 3123–3137.
- Bauer, K.W., Planavsky, N.J., Reinhard, C.T., Cole, D.B., 2021. The Chromium Isotope System as a Tracer of Ocean and Atmosphere Redox. Cambridge University
- Blättler, C.L., Miller, N.R., Higgins, J.A., 2015. Mg and Ca isotope signatures of authigenic dolomite in siliceous deep-sea sediments. Earth Planet. Sci. Lett. 419, 32–42.
- Bold, U., Ahm, A.S.C., Schrag, D.P., Higgins, J.A., Jamsran, E., Macdonald, F.A., 2020. Effect of dolomitization on isotopic records from Neoproterozoic carbonates in southwestern Mongolia. Precamb. Res. 350. 105902.
- Boonchayaanant, B., Gu, B., Wang, W., Ortiz, M.E., Criddle, C.S., 2010. Can microbially-generated hydrogen sulfide account for the rates of U(VI) reduction by a sulfate-reducing bacterium? Biodegradation 21, 81–95.

- Brennecka, G.A., Herrmann, A.D., Algeo, T.J., Anbar, A.D., 2011. Rapid expansion of oceanic anoxia immediately before the end-Permian mass extinction. Proc. Natl. Acad. Sci. U.S.A. 108, 17631–17634.
- Bruske, A., Weyer, S., Zhao, M.Y., Planavsky, N.J., Wegwerth, A., Neubert, N., Dellwig, O., Lau, K.V., Lyons, T.W., 2020. Correlated molybdenum and uranium isotope signatures in modern anoxic sediments: Implications for their use as paleoredox proxy. Geochim. Cosmochim. Acta 270, 449–474.
- Bryant, R.N., Present, T.M., Ahm, A.-S.-C., McClelland, H.-L.-O., Razionale, D., Blättler, C.L., 2022. Early diagenetic constraints on Permian seawater chemistry from the Capitan Reef. Geochim. Cosmochim. Acta 328, 1–18.
- Canfield, D.E., 2013. Sulfur isotopes in coal constrain the evolution of the Phanerozoic sulfur cycle. Proc. Natl. Acad. Sci. U.S.A. 110, 8443–8446.
- Canfield, D., Thamdrup, B., 2009. Towards a consistent classification scheme for geochemical environments, or, why we wish the term 'suboxic'would go away. Geobiology 7, 385–392.
- Cantine, M.D., Knoll, A.H., Bergmann, K.D., 2020. Carbonates before skeletons: A database approach. Earth-Sci. Rev. 201. 103065.
- Chen, Z.Q., Benton, M.J., 2012. The timing and pattern of biotic recovery following the end-Permian mass extinction. Nat. Geosci. 5, 375–383.
- Chen, X., Romaniello, S.J., Herrmann, A.D., Hardisty, D., Gill, B.C., Anbar, A.D., 2018. Diagenetic effects on uranium isotope fractionation in carbonate sediments from the Bahamas. Geochim. Cosmochim. Acta 237, 294–311.
- Chen, X., Tissot, F.L.H., Jansen, M.F., Bekker, A., Liu, C.X., Nie, N.X., Halverson, G.P., Veizer, J., Dauphas, N., 2021. The uranium isotopic record of shales and carbonates through geologic time. Geochim. Cosmochim. Acta 300, 164–191.
- Clarkson, M.O., Musing, K., Andersen, M.B., Vance, D., 2020. Examining pelagic carbonate-rich sediments as an archive for authigenic uranium and molybdenum isotopes using reductive cleaning and leaching experiments. Chem. Geol. 539, 119412.
- Crockford, P.W., Kunzmann, M., Blattler, C.L., Kalderon-Asael, B., Murphy, J.G., Ahm, A.S., Sharoni, S., Halverson, G.P., Planavsky, N.J., Halevy, I., Higgins, J.A., 2021. Reconstructing Neoproterozoic seawater chemistry from early diagenetic dolomite. Geology 49, 442–446.
- Cui, Y., Bercovici, A., Yu, J.X., Kump, L.R., Freeman, K.H., Su, S.G., Vajda, V., 2017. Carbon cycle perturbation expressed in terrestrial Permian-Triassic boundary sections in South China. Global Planet. Change 148, 272–285.
- Dellinger, M., Hardisty, D.S., Planaysky, N.J., Gill, B.C., Kalderon-Asael, B., Asael, D., Croissant, T., Swart, P.K., West, A.J., 2020. The effects of diagenesis on lithium isotope ratios of shallow marine carbonates. Am. J. Sci. 320, 150–184.
- Derry, L.A., 2010. A burial diagenesis origin for the Ediacaran Shuram-Wonoka carbon isotope anomaly. Earth Planet. Sci. Lett. 294, 152–162.
- Droxler, A.W., Schlager, W., 1985. Glacial versus interglacial sedimentation-rates and turbidite frequency in the Bahamas. Geology 13, 799–802.
- Droxler, A.W., Schlager, W., Whallon, C.C., 1983. Quaternary aragonite cycles and oxygen-isotope record in Bahamian carbonate ooze. Geology 11, 235–239.
- Fantle, M.S., DePaolo, D.J., 2007. Ca isotopes in carbonate sediment and pore fluid from ODP Site 807A: the Ca<sup>2+</sup>(aq)-calcite equilibrium fractionation factor and calcite recrystallization rates in Pleistocene sediments. Geochim. Cosmochim. Acta 71, 2524–2546.
- Fantle, M.S., Barnes, B.D., Lau, K.V., 2020. (2020) The Role of Diagenesis in Shaping the Geochemistry of the Marine Carbonate Record. Annu. Rev. Earth Planet. Sci. 48 (48), 549–583.
- Fantle, M.S., Higgins, J., 2014. The effects of diagenesis and dolomitization on Ca and Mg isotopes in marine platform carbonates: Implications for the geochemical cycles of Ca and Mg. Geochim. Cosmochim. Acta 142, 458–481.
- Froelich, P.N., Klinkhammer, G., Bender, M.A.A., Luedtke, N., Heath, G.R., Cullen, D., Dauphin, P., Hammond, D., Hartman, B., Maynard, V., 1979. Early oxidation of organic matter in pelagic sediments of the eastern equatorial Atlantic: suboxic diagenesis. Geochim. Cosmochim. Acta 43, 1075–1090.
- Gill, B.C., Lyons, T.W., Frank, T.D., 2008. Behavior of carbonate-associated sulfate during meteoric diagenesis and implications for the sulfur isotope paleoproxy. Geochim. Cosmochim. Acta 72, 4699–4711.
- Gill, B.C., Lyons, T.W., Young, S.A., Kump, L.R., Knoll, A.H., Saltzman, M.R., 2011. Geochemical evidence for widespread euxinia in the Later Cambrian ocean. Nature 469, 80–83.
- Gilleaudeau, G.J., Romanielloh, S.J., Luo, G.M., Kaufman, A.J., Zhang, F.F., Klaebe, R.M., Kah, L.C., Azmy, K., Bartley, J.K., Zheng, W., Knoll, A.H., Anbar, A.D., 2019. Uranium isotope evidence for limited euxinia in mid-Proterozoic oceans. Earth Planet. Sci. Lett. 521, 150–157.
- Gussone, N., Böhm, F., Eisenhauer, A., Dietzel, M., Heuser, A., Teichert, B.M., Reitner, J., Wörheide, G., Dullo, W.-C., 2005. Calcium isotope fractionation in calcite and aragonite. Geochim. Cosmochim. Acta 69, 4485–4494.
- Gussone, N., Ahm, A.S.C., Lau, K.V., Bradbury, H.J., 2020. Calcium isotopes in deep time: Potential and limitations. Chem. Geol. 544. 119601.
- Hardie, L.A., 1996. Secular variation in seawater chemistry: An explanation for the coupled secular variation in the mineralogies of marine limestones and potash evaporites over the past 600 my. Geology 24, 279–283.
- evaporites over the past 600 my. Geology 24, 279–283.

  Hardisty, D.S., Lu, Z., Bekker, A., Diamond, C.W., Gill, B.C., Jiang, G., Kah, L.C., Knoll, A. H., Loyd, S.J., Osburn, M.R., Planavsky, N.J., Wang, C., Zhou, X., Lyons, T.W., 2017.

  Perspectives on Proterozoic surface ocean redox from iodine contents in ancient and recent carbonate. Earth Planet. Sci. Lett. 463, 159–170.
- Hardisty, D.S., Lyons, T.W., Riedinger, N., Isson, T.T., Owens, J.D., Aller, R.C., Rye, D.M., Planavsky, N.J., Reinhard, C.T., Gill, B.G., Masterson, A.L., Asael, D., Johnston, D.T., 2018. An evaluation of sedimentary molybdenum and iron as proxies for pore fluid paleoredox conditions. Am. J. Sci. 318, 527–556.

- Hayes, J.M., Waldbauer, J.R., 2006. The carbon cycle and associated redox processes through time. Philos. Trans. R. Soc. B: Biol. Sci. 361, 931–950.
- Herrmann, A.D., Gordon, G.W., Anbar, A.D., 2018. Uranium isotope variations in a dolomitized Jurassic carbonate platform (Tithonian; Franconian Alb, Southern Germany). Chem. Geol. 497, 41–53.
- Higgins, J., Schrag, D., 2012. Records of Neogene seawater chemistry and diagenesis in deep-sea carbonate sediments and pore fluids. Earth Planet. Sci. Lett. 357, 386–396.
- Higgins, J., Blättler, C., Lundstrom, E., Santiago-Ramos, D., Akhtar, A., Ahm, A.C., Bialik, O., Holmden, C., Bradbury, H., Murray, S., 2018. Mineralogy, early marine diagenesis, and the chemistry of shallow-water carbonate sediments. Geochim. Cosmochim. Acta 220, 512–534.
- Higgins, J., Schrag, D., 2010. Constraining magnesium cycling in marine sediments using magnesium isotopes. Geochim. Cosmochim. Acta 74, 5039–5053.
- Himmler, T., Bach, W., Bohrmann, G., Peckmann, J., 2010. Rare earth elements in authigenic methane-seep carbonates as tracers for fluid composition during early diagenesis. Chem. Geol. 277, 126–136.
- Holmden, C., Jacobson, A.D., Sageman, B.B., Hurtgen, M.T., 2016. Response of the Cr isotope proxy to Cretaceous Ocean Anoxic Event 2 in a pelagic carbonate succession from the Western Interior Seaway. Geochim. Cosmochim. Acta 186, 277–295.
- Holmden, C., Papanastassiou, D.A., Blanchon, P., Evans, S., 2012. δ<sup>44/40</sup>Ca variability in shallow water carbonates and the impact of submarine groundwater discharge on Ca-cycling in marine environments. Geochim. Cosmochim. Acta 83, 179–194.
- Hood, A.V.S., Planavsky, N.J., Wallace, M.W., Wang, X., Bellefroid, E.J., Gueguen, B., Cole, D.B., 2016. Integrated geochemical-petrographic insights from component-selective 8<sup>238</sup>U of Cryogenian marine carbonates. Geology 44, 935–938.
- Hood, A.V.S., Planavsky, N.J., Wallace, M.W., Wang, X., 2018. The Effects of Diagenesis on Geochemical Paleoredox Proxies in Sedimentary Carbonates. Geochim. Cosmochim. Acta 232, 265–287.
- Horacek, M., Brandner, R., Abart, R., 2007. Carbon isotope record of the P/T boundary and the Lower Triassic in the Southern Alps: Evidence for rapid changes in storage of organic carbon. Palaeogeogr. Palaeoclim. Palaeoecol. 252, 347–354.
- Hua, B., Xu, H., Terry, J., Deng, B., 2006. Kinetics of uranium(VI) reduction by hydrogen sulfide in anoxic aqueous systems. Environ. Sci. Technol. 40, 4666– 4671.
- Hülse, D., Lau, K.V., van de Velde, S.J., Arndt, S., Meyer, K.M., Ridgwell, A., 2021. End-Permian marine extinction due to temperature-driven nutrient recycling and euxinia. Nat. Geosci. 14, 862–867.
- Husson, J.M., Higgins, J.A., Maloof, A.C., Schoene, B., 2015. Ca and Mg isotope constraints on the origin of Earth's deepest  $\delta^{13}$ C excursion. Geochim. Cosmochim. Acta 160, 243–266.
- Jacobsen, S.B., Kaufman, A.J., 1999. The Sr, C and O isotopic evolution of Neoproterozoic seawater. Chem. Geol. 161, 37–57.
- Jia-Zhong, Z., Whitfield, M., 1986. Kinetics of inorganic redox reactions in seawater: I. The reduction of iodate by bisulphide. Mar. Chem. 19, 121–137.
- Joachimski, M.M., Lai, X.L., Shen, S.Z., Jiang, H.S., Luo, G.M., Chen, B., Chen, J., Sun, Y. D., 2012. Climate warming in the latest Permian and the Permian-Triassic mass extinction. Geology 40, 195–198.
- Joachimski, M.M., Alekseev, A.S., Grigoryan, A., Gatovsky, Y.A., 2020. Siberian Trap volcanism, global warming and the Permian-Triassic mass extinction: New insights from Armenian Permian-Triassic sections. Geol. Soc. Am. Bull. 132, 427–443.
- Jones, D.S., Brothers, R.W., Ahm, A.S.C., Slater, N., Higgins, J.A., Fike, D.A., 2020. Sea level, carbonate mineralogy, and early diagenesis controlled  $\delta^{13}$ C records in Upper Ordovician carbonates. Geology 48, 194–199.
- Kennedy, H., Elderfield, H., 1987a. Iodine diagenesis in non-pelagic deep-sea sediments. Geochim. Cosmochim. Acta 51, 2505–2514.
- Kennedy, H., Elderfield, H., 1987b. Iodine diagenesis in pelagic deep-sea sediments. Geochim. Cosmochim. Acta 51, 2489–2504.
- Kenter, J.A., Ginsburg, R., Troelstra, N., Simon, R., 2001. Sea-level-driven sedimentation patterns on the slope and margin. SEPM Sp. Pub. 70, 61–100.
- Kinsman, D.J.J., 1969. Interpretation of Sr+2 concentrations in carbonate minerals and rocks. J. Sediment. Petrol. 39, 486–508.
- Kinsman, D.J., Holland, H.D., 1969. The co-precipitation of cations with  $CaCO_3$ —IV. The co-precipitation of  $Sr^{2+}$  with aragonite between  $16^\circ$  and  $96^\circ$  C. Geochim. Cosmochim. Acta 33, 1-17.
- Komar, N., Zeebe, R.E., 2016. Calcium and calcium isotope changes during carbon cycle perturbations at the end-Permian. Paleoceanography 31, 115–130.
- Kramer, P.A., Swart, P.K., De Carlo, E.H., Schovsbo, N.H., 2000. Overview of interstitial fluid and sediment geochemistry, sites 1003–1007 (Bahamas transect). Proc. ODP Sci. Results 166, 179–195.
- Krissansen-Totton, J., Buick, R., Catling, D.C., 2015. A statistical analysis of the carbon isotope record from the archean to phanerozoic and implications for the rise of oxygen. Am. J. Sci. 315, 275–316.
- Lau, K.V., Maher, K., Altiner, D., Kelley, B.M., Kump, L.R., Lehrmann, D.J., Silva-Tamayo, J.C., Weaver, K.L., Yu, M.Y., Payne, J.L., 2016. Marine anoxia and delayed Earth system recovery after the end-Permian extinction. Proc. Natl. Acad. Sci. U. S.A. 113, 2360–2365.
- Lau, K.V., Maher, K., Brown, S.T., Jost, A.B., Altiner, D., DePaolo, D.J., Eisenhauer, A., Kelley, B.M., Lehrmann, D.J., Paytan, A., Yu, M., Silva-Tamayo, J.C., Payne, J.L., 2017. The influence of seawater carbonate chemistry, mineralogy, and diagenesis on calcium isotope variations in Lower-Middle Triassic carbonate rocks. Chem. Geol. 471, 13–37.

- Lau, K.V., Romaniello, S.J., Zhang, F., 2019. The Uranium Isotope Paleoredox Proxy. Cambridge University Press.
- Li, C., Hardisty, D.S., Luo, G., Huang, J., Algeo, T.J., Cheng, M., Shi, W., An, Z., Tong, J., Xie, S., 2017. Uncovering the spatial heterogeneity of Ediacaran carbon cycling. Geobiology 15, 211–224.
- Liu, X.-M., Hardisty, D.S., Lyons, T.W., Swart, P.K., 2019. Evaluating the fidelity of the cerium paleoredox tracer during variable carbonate diagenesis on the Great Bahamas Bank. Geochim. Cosmochim. Acta 248, 25–42.
- Lu, Z., Lu, W., Rickaby, R.E., Thomas, E., 2020. Earth History of Oxygen and the iprOxy. Cambridge University Press.
- Lyons, T.W., Walter, L.M., Gellatly, A.M., Martini, A.M., Blake, R.E., 2004. Sites of anomalous organic remineralization in the carbonate sediments of South Florida, USA: the sulfur cycle and carbonate-associated sulfate. Geol. Soc. Am. Sp. Pap. 379, 161–176.
- Mackenzie, F.T., Morse, J.W., 1992. Sedimentary carbonates through Phanerozoic time. Geochim. Cosmochim. Acta 56, 3281–3295.
- McClain, C.N., Maher, K., 2016. Chromium fluxes and speciation in ultramafic catchments and global rivers. Chem. Geol. 426, 135–157.
- McClain, M.E., Swart, P.K., Vacher, H.L., 1992. The hydrogeochemistry of early meteoric diagenesis in a Holocene deposit of biogenic carbonates. J. Sediment. Res. 62.
- Meece, D.E., Benninger, L.K., 1993. The coprecipitation of Pu and other radionuclides with CaCO<sub>3</sub>. Geochim. Cosmochim. Acta 57, 1447–1458.
- Melim, L.A., 1996. Limitations on lowstand meteoric diagenesis in the Pliocene-Pleistocene of Florida and Great Bahama Bank: Implications for eustatic sealevel models. Geology 24, 893–896.
- Melim, L.A., Swart, P.K., Maliva, R.G., 1995. Meteoric-like fabrics forming in marine waters: implications for the use of petrography to identify diagenetic environments. Geology 23, 755–758.
- Melim, L.A., Swart, P.K., Eberli, G.P., 2004. Mixing-zone diagenesis in the subsurface of Florida and the Bahamas. J. Sediment. Res. 74, 904–913.
- Meyer, K.M., Yu, M., Lehrmann, D., van de Schootbrugge, B., Payne, J.L., 2013. Constraints on Early Triassic carbon cycle dynamics from paired organic and inorganic carbon isotope records. Earth Planet. Sci. Lett. 361, 429–435.
- Murray, S.T., Higgins, J.A., Holmden, C., Lu, C.J., Swart, P.K., 2021. Geochemical fingerprints of dolomitization in Bahamian carbonates: Evidence from sulphur, calcium, magnesium and clumped isotopes. Sedimentology 68, 1–29.
- Nelson, L.L., Ahm, A.S.C., Macdonald, F.A., Higgins, J.A., Smith, E.F., 2021. Fingerprinting local controls on the Neoproterozoic carbon cycle with the isotopic record of Cryogenian carbonates in the Panamint Range, California. Earth Planet. Sci. Lett. 566. 116956.
- Oehlert, A.M., Swart, P.K., 2014. Interpreting carbonate and organic carbon isotope covariance in the sedimentary record. Nat. Comm. 5, 1–7.
- Oehtert, A.M., Swart, P.K., 2019. Rolling window regression of  $\delta^{13}C$  and  $\delta^{18}O$  values in carbonate sediments: Implications for source and diagenesis. Deposit. Rec. 5, 613–630.
- Owens, J.D., Gill, B.C., Jenkyns, H.C., Bates, S.M., Severmann, S., Kuypers, M.M.M., Woodfine, R.G., Lyons, T.W., 2013. Sulfur isotopes track the global extent and dynamics of euxinia during Cretaceous Oceanic Anoxic Event 2. Proc. Natl. Acad. Sci. U.S.A. 110, 18407–18412.
- Payne, J.L., Lehrmann, D.J., Wei, J.Y., Orchard, M.J., Schrag, D.P., Knoll, A.H., 2004. Large perturbations of the carbon cycle during recovery from the end-Permian extinction. Science 305, 506–509.
- Payne, J.L., Lehrmann, D.J., Follett, D., Seibel, M., Kump, L.R., Riccardi, A., Altiner, D., Sano, H., Wei, J., 2007. Erosional truncation of uppermost Permian shallow-marine carbonates and implications for Permian-Triassic boundary events. Geol. Soc. Am. Bull. 119, 771–784.
- Payne, J.L., Turchyn, A.V., Paytan, A., DePaolo, D.J., Lehrmann, D.J., Yu, M.Y., Wei, J.Y., 2010. Calcium isotope constraints on the end-Permian mass extinction. Proc. Natl. Acad. Sci. U.S.A. 107, 8543–8548.
- Pettine, M., Millero, F.J., Passino, R., 1994. Reduction of chromium(VI) with hydrogen-sulfide in NaCl media. Mar. Chem. 46, 335–344. Present, T.M., Adkins, J.F., Fischer, W.W., 2020. Variability in Sulfur Isotope Records
- Present, T.M., Adkins, J.F., Fischer, W.W., 2020. Variability in Sulfur Isotope Records of Phanerozoic Seawater Sulfate. Geophys. Res. Lett. 47. e2020GL088766.Present, T.M., Paris, G., Burke, A., Fischer, W.W., Adkins, J.F., 2015. Large Carbonate
- Present, T.M., Paris, G., Burke, A., Fischer, W.W., Adkins, J.F., 2015. Large Carbonate Associated Sulfate isotopic variability between brachiopods, micrite, and other sedimentary components in Late Ordovician strata. Earth Planet. Sci. Lett. 432, 187–198.
- Present, T.M., Gutierrez, M., Paris, G., Kerans, C., Grotzinger, J.P., Adkins, J.F., 2019. Diagenetic controls on the isotopic composition of carbonate-associated sulphate in the Permian Capitan Reef Complex, West Texas. Sedimentology 66. 2605–2626.
- Richardson, J.A., Keating, C., Lepland, A., Hints, O., Bradley, A.S., Fike, D.A., 2019. Silurian records of carbon and sulfur cycling from Estonia: The importance of depositional environment on isotopic trends. Earth Planet. Sci. Lett. 512, 71–82.
- Romaniello, S.J., Herrmann, A.D., Anbar, A.D., 2013. Uranium concentrations and <sup>238</sup>U/<sup>235</sup>U isotope ratios in modern carbonates from the Bahamas: Assessing a novel paleoredox proxy. Chem. Geol. 362, 305–316.

- Schlager, W., Reijmer, J.J.G., Droxler, A., 1994. Highstand shedding of carbonate platforms. J. Sediment. Res. 64, 270–281.
- Schobben, M., Joachimski, M.M., Korn, D., Leda, L., Korte, C., 2014. Palaeotethys seawater temperature rise and an intensified hydrological cycle following the end-Permian mass extinction. Gondwana Res. 26, 675–683.
- Silva-Tamayo, J.C., Lau, K.V., Jost, A.B., Payne, J.L., Wignall, P.B., Newton, R.J., Eisenhauer, A., Depaolo, D.J., Brown, S., Maher, K., Lehrmann, D.J., Altiner, D., Yu, M.Y., Richoz, S., Paytan, A., 2018. Global perturbation of the marine calcium cycle during the Permian-Triassic transition. Geol. Soc. Am. Bull. 130, 1323– 1338.
- Smrzka, D., Zwicker, J., Bach, W., Feng, D., Himmler, T., Chen, D., Peckmann, J., 2019. The behavior of trace elements in seawater, sedimentary pore water, and their incorporation into carbonate minerals: a review. Facies, 65.
- Song, H.Y., Tong, J.N., Algeo, T.J., Song, H.J., Qiu, H.O., Zhu, Y.Y., Tian, L., Bates, S., Lyons, T.W., Luo, G.M., Kump, L.R., 2014. Early Triassic seawater sulfate drawdown. Geochim. Cosmochim. Acta 128, 95–113.
- Stanley, S.M., Hardie, L.A., 1998. Secular oscillations in the carbonate mineralogy of reef-building and sediment-producing organisms driven by tectonically forced shifts in seawater chemistry. Palaeogeogr. Palaeoclimat. Palaeoecol. 144, 3–19.
- Stewart, J.A., Gutjahr, M., Pearce, F., Swart, P.K., Foster, G.L., 2015. Boron during meteoric diagenesis and its potential implications for Marinoan snowball Earth  $\delta^{11}$ B-pH excursions. Geology 43, 627–630.
- Swart, P.K., Eberli, G., 2005. The nature of the  $\delta^{13}$ C of periplatform sediments: implications for stratigraphy and the global carbon cycle. Sediment. Geol. 175, 115–129.
- Swart, P.K., Melim, L.A., 2000. The origin of dolomites in Tertiary sediments from the margin of Great Bahama Bank. J. Sediment. Res. 70, 738–748.
   Swart, P.K., Elderfield, H., Beets, K., 2001. The <sup>87</sup>Sr/<sup>86</sup>Sr ratios of carbonates,
- Swart, P.K., Elderfield, H., Beets, K., 2001. The "Sr/PoSr ratios of carbonates, phosphorites, and fluids collected during the Bahamas drilling project cores Clino and Unda: implications for dating and diagenesis. SEPM Sp. Pub. 70, 175–185.
- Swart, P.K., Oehlert, A.M., 2018. Revised interpretations of stable C and O patterns in carbonate rocks resulting from meteoric diagenesis. Sediment. Geol. 364, 14–23
- Tipper, E.T., 2022. Magnesium Isotopes: Tracer for the Global Biogeochemical Cycle of Magnesium Past and Present or Archive of Alteration? Cambridge University Press.
- Tissot, F.L.H., Chen, C., Go, B.M., Naziemiec, M., Healy, G., Bekker, A., Swart, P.K., Dauphas, N., 2018. Controls of eustasy and diagenesis on the <sup>238</sup>U/<sup>235</sup>U of carbonates and evolution of the seawater (<sup>234</sup>U/<sup>238</sup>U) during the last 1.4 Myr. Geochim. Cosmochim. Acta 242, 233–265.
- Tostevin, R., 2021. Cerium anomalies and paleoredox. Cambridge University Press.
- Tostevin, R., Shields, G.A., Tarbuck, G.M., He, T., Clarkson, M.O., Wood, R.A., 2016. Effective use of cerium anomalies as a redox proxy in carbonate-dominated marine settings. Chem. Geol. 438, 146–162.
- Tromp, T.K., Vancappellen, P., Key, R.M., 1995. A global-model for the early diagenesis of organic carbon and organic phosphorus in marine-sediments. Geochim. Cosmochim. Acta 59, 1259–1284.
- Tucker, M.E., 1982. Precambrian dolomites: petrographic and isotopic evidence that they differ from Phanerozoic dolomites. Geology 10, 7–12.
- Upstillgoddard, R.C., Elderfield, H., 1988. The role of diagenesis in the estuarine budgets of iodine and bromine. Continental Shelf Res. 8, 405–430.
- Wang, J.Y., Jacobson, A.D., Zhang, H., Ramezani, J., Sageman, B.B., Hurtgen, M.T., Bowring, S.A., Shen, S.Z., 2019. Coupled δ<sup>44/40</sup>Ca, δ<sup>88/86</sup>Sr, and <sup>87</sup>Sr/<sup>86</sup>Sr geochemistry across the end-Permian mass extinction event. Geochim. Cosmochim. Acta 262, 143–165.
- Wang, C.L., Reinhard, C.T., Rybacki, K.S., Hardisty, D.S., Ossa, F.O., Wang, X.L., Hofmann, A., Asael, D., Robbins, L.J., Zhang, L.C., Planavsky, N.J., 2021. Chromium isotope systematics and the diagenesis of marine carbonates. Earth Planet. Sci. Lett. 562
- Zhang, F., Xiao, S., Romaniello, S.J., Hardisty, D., Li, C., Melezhik, V., Pokrovsky, B., Cheng, M., Shi, W., Lenton, T.M., Anbar, A.D., 2019. Global marine redox changes drove the rise and fall of the Ediacara biota. Geobiology 17, 594–610.
- Zhang, F., Lenton, T.M., del Rey, A., Romaniello, S.J., Chen, X., Planavsky, N.J., Clarkson, M.O., Dahl, T.W., Lau, K.V., Wang, W., Li, Z., Zhao, M., Isson, T., Algeo, T.J., Anbar, A.D., 2020. Uranium isotopes in marine carbonates as a global ocean paleoredox proxy: A critical review. Geochim. Cosmochim. Acta 287, 27–49.
- Zhang, F.F., Romaniello, S.J., Algeo, T.J., Lau, K.V., Clapham, M.E., Richoz, S., Herrmann, A.D., Smith, H., Horacek, M., Anbar, A.D., 2018. Multiple episodes of extensive marine anoxia linked to global warming and continental weathering following the latest Permian mass extinction. Sci. Adv. 4.
- Zhao, M.Y., Planavsky, N., Oehlert, A.M., Wei, G.Y., Gong, Z., 2020. Simulating meteoric and mixing zone carbonate diagenesis with a two-dimensional reactive transport model. Am. J. Sci. 320, 599–636.